

ALMA MATER STUDIORUM · UNIVERSITY OF BOLOGNA

School of Science
Department of Physics and Astronomy
Master Degree in Physics

Exploring the muon-Higgs coupling at a multi-TeV muon collider

Supervisor
Prof. Davide Pagani

Co-supervisor
Prof. Fabio Maltoni

Submitted by
Eugenia Celada

Academic Year 2021/2022

Abstract

We investigate the potential of a high-energy muon collider in measuring the muon Yukawa coupling (y_μ) in the production of two, three and four heavy bosons via muon-antimuon annihilations. We study the sensitivity of these processes to deviations of y_μ from the Standard Model prediction, parametrized by an effective dimension-6 operator in the Standard Model Effective Field Theory (SMEFT) framework. We also consider the κ framework, in which the deviation is simply parametrized by a strength modification of the $\mu^+\mu^-h$ vertex alone. Both frameworks lead to an energy enhancement of the cross sections with one or more vector bosons, although the κ framework yields stronger effects, especially for the production of four bosons. On the contrary, for purely-Higgs final states the cross section is suppressed in the κ framework, while it is extremely sensitive to deviations in the SMEFT. We show that the triple-Higgs production is the most sensitive process to spot new physics effects on y_μ .

Contents

Introduction	3
1 The Standard Model	5
1.1 The electroweak Standard Model Lagrangian	6
1.1.1 Electroweak Symmetry Breaking mechanism	7
1.1.2 Fermion sector	9
1.1.3 Yukawa sector	11
1.2 Unitarity cancellations in the SM	12
1.2.1 Goldstone Boson Equivalence theorem	12
1.2.2 High-energy behavior in $\mu^+\mu^- \rightarrow ZZ$	13
2 Investigating the Higgs couplings	19
2.1 Overview on Higgs couplings measurements	19
2.1.1 Higgs interactions at LHC	19
2.1.2 Future perspectives	20
2.2 The muon Yukawa coupling	21
2.2.1 Muon anomalies	22
2.2.2 Muon colliders	25
3 Theoretical frameworks	28
3.1 The SMEFT and κ formalisms	28
3.1.1 The Effective Field Theory approach	28
3.1.2 The κ framework	31
3.2 Muon Yukawa coupling in SMEFT	32
3.2.1 Feynman rules	33
3.2.2 EFT vs κ framework	35
4 Multiboson production	38
4.1 Perturbative expansion in the effective coupling	39
4.1.1 First order suppression	40
4.1.2 Second order is dominant	44

4.2	High-energy behavior for multiboson production	46
4.2.1	Analytical predictions	47
4.2.2	Numerical results	50
4.3	Results	52
4.3.1	EFT framework	52
4.3.2	κ framework	54
	Conclusions	56
	Appendix	58

Introduction

After a century of continuous theoretical and experimental progress, the research for a theory of fundamental interactions culminated in the formulation of the Standard Model, which describes electromagnetic, weak and strong forces in terms of a $SU(3) \times SU(2) \times U(1)$ gauge theory. The last missing particle was the Higgs boson, which was predicted by the Electroweak Symmetry Breaking mechanism, and it was finally observed in 2012 [1],[2]. Despite the abundance of experimental confirmations at colliders, there is clear evidence that this cannot be the ultimate theory and that some physics beyond the Standard Model is needed. Dark matter, the generation of neutrino masses, or the matter/antimatter asymmetry, are just some examples of the physics that are awaiting for a deeper description.

Nevertheless, at the moment we are lacking specific indications on where to look for new physics, suggesting that it probably lies beyond the present energy reach at colliders. In absence of well-defined traces, the study of the Higgs sector holds the greatest potential for discoveries. Indeed, the precision that has been reached so far on the Higgs couplings measurements still leaves room for deviations from the Standard Model predictions, paving the way for a more fundamental theory. In particular, the Higgs coupling to light flavors has not been probed yet, apart from the muon coupling which has been measured with a large uncertainty [3],[4]. In this situation, two different paths are possible at colliders: increasing the precision, in order to detect indirect effects of heavy physics, or increasing the energy reach to access the new states directly. Both approaches require the construction of a new collider.

In this work, motivated by the proposal of a future high-energy muon collider and by recent developments in muon physics, we study the sensitivity to the muon Yukawa coupling in the production of multiple heavy bosons (W^\pm , Z^0 and h) via muon-antimuon annihilations. The thesis is organised as follows. In chapter 1 we review the basic features of the Standard Model, with a specific focus on the Higgs role in preserving unitarity. Chapter 2 presents an overview of the current experimental status on the Higgs coupling measurements, and some motivations for the study of the muon Yukawa coupling. In chapter 3 we discuss the parametrization of new physics into two frameworks, the Standard Model Effective Field Theory (SMEFT) and the κ framework, focusing in particular on a dimension-6 operator in SMEFT. Finally, in chapter 4 we study in detail

the multiboson production processes in the SMEFT and κ frameworks, with a particular emphasis on the high-energy limit, presenting our results.

Chapter 1

The Standard Model

The present knowledge of fundamental interactions is summarised in an elegant and compact formulation, the Standard Model (SM), predicting with impressive accuracy most of the experimental data at colliders. In this description, strong and electroweak interactions are described in terms of a $SU(3)_C \times SU(2)_L \times U(1)_Y$ gauge invariant quantum field theory, where the electroweak sector $SU(2)_L \times U(1)_Y$ is spontaneously broken by the Higgs mechanism.

According to this picture, matter is described by fermionic quantum fields, and their interactions are mediated by vectorial gauge bosons. The interaction of matter with the scalar Higgs boson has different nature and provides the masses to fermions and to the weak interaction's mediators W^\pm and Z^0 .

Finally, the SM depends on 19 free parameters (assuming the neutrino massless):

- 9 fermion masses,
- 3 angles and 1 phase of the Cabibbo-Kobayashi-Maskawa (CKM) matrix,
- the strong coupling constant α_s and the QCD Landau pole,
- the Higgs mass,
- 3 electroweak parameters, chosen among the fine structure constant α , the Fermi constant G_F and the gauge boson masses m_Z and m_W .

Once measured, these parameters allow to extract theoretical predictions and so far they are providing a spectacular agreement with experimental results at colliders.

However, the Standard Model carries several unexplained features, open questions and technical issues, suggesting that this description is far from being complete. For example, the SM does not provide a mass term for neutrinos, a quantum formulation of gravity, an explanation for dark matter, the asymmetry between matter and antimatter in the

Universe, just to cite some of them. All these limitations indicate the need for a more fundamental theory.

In the first section of this chapter we briefly discuss the structure of the electroweak sector of the SM and the Electroweak Symmetry Breaking (EWSB) mechanism. The second section is devoted to a fundamental property of the SM, which is the unitarization of matrix elements at high energies, in which the Higgs field plays a central role. The role of the Higgs interaction with fermions in preserving unitarity will be the foundation of the phenomenological analysis carried out further in this work.

1.1 The electroweak Standard Model Lagrangian

Symmetries are the guiding principle to build the SM Lagrangian. Besides Lorentz invariance, all operators must respect the gauge $SU(3)_C \times SU(2)_L \times U(1)_Y$ symmetry. This is schematically realised by substituting the ordinary partial derivative in the free Lagrangian with the gauge-covariant derivative, defined as

$$D_\mu = \partial_\mu - igU_\mu^a t^a. \quad (1.1)$$

It contains new vector fields U_μ^a in the same number as the generators of the gauge group t^a . They are called gauge fields and mediate interactions by coupling to matter with strength g . The gauge invariance condition is sufficiently strict to uniquely determine the 4-dimensional operators describing gauge interactions. This description still misses an important feature of the SM: in fact, a gauge invariant mass term for gauge bosons and fermions cannot be written within this theory. The problem is solved by introducing a scalar field, the Higgs, that generates the masses thanks to the Spontaneous Symmetry Breaking (SSB) mechanism.

The SM Lagrangian can be separated into a QCD sector \mathcal{L}_{EW} and an electroweak sector:

$$\mathcal{L}_{\text{SM}} = \mathcal{L}_{\text{QCD}} + \mathcal{L}_{\text{EW}} = \mathcal{L}_{\text{QCD}} + \mathcal{L}_{\text{EW}}^{\text{fermions}} + \mathcal{L}_{\text{EW}}^{\text{gauge}} + \mathcal{L}_{\text{EW}}^{\text{Higgs}} + \mathcal{L}_{\text{Yukawa}}. \quad (1.2)$$

The EW Lagrangian contains the following terms:

- $\mathcal{L}_{\text{EW}}^{\text{gauge}}$ contains the gauge bosons kinetic and self-interaction terms,
- $\mathcal{L}_{\text{EW}}^{\text{fermions}}$ describes the interaction between fermions and electroweak gauge bosons,
- $\mathcal{L}_{\text{EW}}^{\text{Higgs}}$ is the Higgs field kinetic term and potential,
- $\mathcal{L}_{\text{Yukawa}}$ is the Yukawa operator, involving the Higgs and fermion fields. After spontaneous symmetry breaking, it generates the interaction between fermions and Higgs boson and the fermionic masses.

1.1.1 Electroweak Symmetry Breaking mechanism

The $SU(2)_L \times U(1)_Y$ group is generated by three weak isospin operators I_1, I_2, I_3 and the hypercharge Y . The associated vector fields are a $SU(2)_L$ triplet W_μ^a and an isospin singlet B_μ with hypercharge Y . Denoting respectively with g_1 and g_2 the $U(1)_Y$ and $SU(2)_L$ coupling constants, the gauge bosons part of the Lagrangian is

$$\mathcal{L}_{\text{EW}}^{\text{gauge}} = -\frac{1}{4}W_{\mu\nu}^a W^{\mu\nu a} - \frac{1}{4}B_{\mu\nu}B^{\mu\nu} \quad (1.3)$$

where we have introduced the field strength tensors

$$W_{\mu\nu}^a = \partial_\mu W_\nu^a - \partial_\nu W_\mu^a + g_2 \epsilon^{abc} W_\mu^b W_\nu^c, \quad (1.4)$$

$$B_{\mu\nu} = \partial_\mu B_\nu - \partial_\nu B_\mu. \quad (1.5)$$

The partial spontaneous symmetry breaking (SSB) of the $SU(2)_L \times U(1)_Y$ gauge group is realised by introducing a single $SU(2)_L$ doublet of complex scalars

$$\phi = \begin{pmatrix} \phi^+ \\ \phi^0 \end{pmatrix} \quad (1.6)$$

with hypercharge $Y = 1$ according to the Weinberg relation

$$Q = I_3 + \frac{Y}{2} \quad (1.7)$$

and a potential

$$V(\phi^\dagger \phi) = -\mu^2 \phi^\dagger \phi + \lambda (\phi^\dagger \phi)^2. \quad (1.8)$$

The coupling to the gauge fields is introduced by substituting the derivative ∂_μ with the covariant derivative defined as

$$D_\mu = \partial_\mu - ig_2 I^a W_\mu^a - ig_1 \frac{Y}{2} B_\mu \quad (1.9)$$

in the free Higgs Lagrangian:

$$\mathcal{L}_{\text{EW}}^{\text{Higgs}} = \left| \partial_\mu \phi - ig_2 I^a W_\mu^a \phi - i \frac{g_1}{2} B_\mu \phi \right|^2 - V(\phi^\dagger \phi). \quad (1.10)$$

The potential in eq. (1.8) has a non vanishing, degenerate ground state

$$|\langle \phi \rangle|^2 = \frac{\mu^2}{2\lambda} \equiv \frac{v^2}{2} \quad (1.11)$$

which describes a three-sphere of radius $v/\sqrt{2}$ in the field space, hence all the corresponding field configurations are equivalent. According to the Goldstone theorem, since the

vacuum is 3-dimensional, there are 3 energetically equivalent degrees of freedom, thus 3 massless Goldstone bosons. They will be reabsorbed in 3 of the 4 gauge bosons becoming, after a change of basis, the masses of the W^\pm and Z^0 bosons.

Since all vacuum configurations are equivalent, we can consider as ground state

$$\langle \phi \rangle = \frac{1}{\sqrt{2}} \begin{pmatrix} 0 \\ v \end{pmatrix}, \quad v = \frac{\mu}{\sqrt{\lambda}}. \quad (1.12)$$

As expected from the Goldstone theorem, there is a 1-dimensional subgroup $U(1)_{\text{em}} \subset SU(2)_L \times U(1)_Y$ that leaves the vacuum invariant. In other words

$$\langle \phi \rangle \xrightarrow{SU(2)_L \times U(1)_Y} \langle \phi \rangle' \neq \langle \phi \rangle, \quad (1.13)$$

but

$$\langle \phi \rangle \xrightarrow{U(1)_{\text{em}}} \langle \phi \rangle. \quad (1.14)$$

Since it is generated by the electric charge operator $\hat{Q} = \hat{I}_3 + \hat{Y}/2$, we recognize it as the gauge group of QED.

We choose a linear parametrization of the fluctuations of ϕ around the vacuum:

$$\phi = \frac{1}{\sqrt{2}} \begin{pmatrix} i\sqrt{2}G_+ \\ v + h + iG_z \end{pmatrix}. \quad (1.15)$$

The complex scalar G_+ and the real one G_z are the Goldstone bosons, while h is the physical Higgs field. Because of the gauge invariance of the Lagrangian however, Goldstone bosons can be gauged away and are therefore unphysical. With this choice, called unitary gauge, the doublet takes the simple form

$$\phi = \frac{1}{\sqrt{2}} \begin{pmatrix} 0 \\ v + h \end{pmatrix}. \quad (1.16)$$

The expansion of $\mathcal{L}_{\text{EW}}^{\text{Higgs}} = \mathcal{L}_{\text{kinetic}}^{\text{Higgs}} - V$ in the unitary gauge generates:

- the mass of h , $m_h = \sqrt{2}\mu$, and the cubic and quartic self-interactions of h from V :

$$V = -\lambda \frac{v^4}{4} + \frac{1}{2} 2\mu^2 h^2 + \lambda v h^3 + \frac{\lambda}{4} h^4, \quad (1.17)$$

- the kinetic term of h and the masses of W^\pm, Z^0 from $\mathcal{L}_{\text{kinetic}}^{\text{Higgs}}$:

$$\mathcal{L}_{\text{kinetic}}^{\text{Higgs}} = \frac{1}{2} \partial_\mu h \partial^\mu h + \frac{1}{8} (v + h)^2 \left(g_2^2 W_\mu^a W^{\mu a} - 2g_1 g_2 W_\mu^3 B^\mu + g_1^2 B_\mu B^\mu \right). \quad (1.18)$$

The masses can be found after diagonalisation. This is done by making a change of basis that leads to the physical EW gauge bosons

$$W_\mu^\pm = \frac{1}{\sqrt{2}}(W_\mu^1 \pm iW_\mu^2) \quad \Rightarrow \quad m_W = \frac{g_2 v}{2} \quad (1.19)$$

$$Z_\mu = \cos \theta_w W_\mu^3 - \sin \theta_w B_\mu \quad \Rightarrow \quad m_Z = \frac{m_W}{\cos \theta_w} \quad (1.20)$$

$$A_\mu = \sin \theta_w W_\mu^3 + \cos \theta_w B_\mu \quad \Rightarrow \quad m_\gamma = 0 \quad (1.21)$$

having defined the Weinberg angle θ_w

$$\tan \theta_w \equiv \frac{g_1}{g_2}. \quad (1.22)$$

We recognise the A_μ field as the photon and the W_μ^\pm and Z fields as the weak force mediators. With these definitions, the gauge Lagrangian in eq. (1.3) gives rise to the kinetic terms and interactions between the electroweak bosons:

$$\mathcal{L}_{\text{EW}}^{\text{gauge}} = -\frac{1}{4}F_{\mu\nu}F^{\mu\nu} - \frac{1}{4}Z_{\mu\nu}Z^{\mu\nu} - \frac{1}{2}W_{\mu\nu}^+W^{\mu\nu-} \quad (1.23)$$

where

$$F_{\mu\nu} = \partial_\mu A_\nu - \partial_\nu A_\mu, \quad (1.24)$$

$$Z_{\mu\nu} = \partial_\mu Z_\nu - \partial_\nu Z_\mu, \quad (1.25)$$

$$W_{\mu\nu}^\pm = \partial_\mu W_\nu^\pm - \partial_\nu W_\mu^\pm. \quad (1.26)$$

1.1.2 Fermion sector

We now discuss the coupling of gauge bosons to fermions. Experimentally, the theory of weak interactions is chiral, since the $SU(2)_L$ gauge bosons only couple to left-handed fermions. Indeed fermion fields are distinguished in eigenstates of the chiral operator as left- or right-handed. Left-handed (LH) spinors form $SU(2)_L$ doublets

$$\psi_j^L = \begin{pmatrix} \psi_{j+}^L \\ \psi_{j-}^L \end{pmatrix} \quad (1.27)$$

where j indicates the family, and $\sigma = \pm$ is the component index. Right-handed (RH) spinors are instead $SU(2)_L$ singlets

$$\psi_j^R = \psi_{j+}^R, \psi_{j-}^R. \quad (1.28)$$

Each field is an eigenstate of Y such that Weinberg relation of eq. (1.7) is fulfilled. In Table 1.1 we summarise the $SU(2)_L$ and $U(1)_Y$ charges for the SM fermionic fields of

	I_3	Y	Q
$Q^L = \begin{pmatrix} u^L \\ d^L \end{pmatrix}$	1/2	1/3	2/3
	-1/2	1/3	-1/3
u^R	0	4/3	2/3
d^R	0	-2/3	-1/3
$L^L = \begin{pmatrix} \nu^L \\ e^L \end{pmatrix}$	1/2	-1	0
	-1/2	-1	-1
e^R	0	-2	-1

Table 1.1: Fermionic fields of first generation and their charges under $SU(2)_L$, $U(1)_Y$ and $U(1)_{\text{em}}$.

the first generation, as the charges are the same for all generations. The fermionic Lagrangian is compactly written as

$$\mathcal{L}_{\text{EW}}^{\text{fermion}} = \sum_j \bar{\psi}_j^L i \not{D} \psi_j^L + \sum_{j,\sigma} \bar{\psi}_{j\sigma}^R i \not{D} \psi_{j\sigma}^R. \quad (1.29)$$

Moving to the mass eigenstates basis, it can be written in a more physically meaningful form. Identifying the electric charge as

$$e = g_2 \sin \theta_w = g_1 \cos \theta_w, \quad (1.30)$$

eq. (1.29) can be written in terms of the electromagnetic current J_{em}^μ , and the neutral and charged weak currents $J_W^{\mu\pm}$ and J_Z^μ . As an example we write explicitly the fields of the first generation.

$$\begin{aligned} \mathcal{L}_{\text{EW}}^{\text{fermion}} = & \bar{L}^L i \not{D} L^L + \bar{e}^R i \not{D} e^R + \bar{Q}^L i \not{D} Q^L + \bar{u}^R i \not{D} u^R + \bar{d}^R i \not{D} d^R + \\ & g_2 (W_\mu^+ J_W^{\mu+} + W_\mu^- J_W^{\mu-} + Z_\mu J_Z^\mu) + e A_\mu J_{\text{em}}^\mu \end{aligned} \quad (1.31)$$

where

$$J_W^{\mu+} = \frac{1}{\sqrt{2}} (\bar{\nu}^L \gamma^\mu e^L + \bar{u}^L \gamma^\mu d^L) = (J_W^{\mu-})^\dagger, \quad (1.32)$$

$$\begin{aligned} J_Z^\mu = & \frac{1}{\cos \theta_w} \left[\nu^L \gamma^\mu \frac{1}{2} \nu^L + \bar{e}^L \gamma^\mu \left(-\frac{1}{2} + \sin^2 \theta_w \right) e^L + \bar{e}^R \gamma^\mu \sin^2 \theta_w e^R \right. \\ & + \bar{u}^L \gamma^\mu \left(\frac{1}{2} - \frac{2}{3} \sin^2 \theta_w \right) u^L + \bar{u}^R \gamma^\mu \left(-\frac{2}{3} \sin^2 \theta_w \right) u^R \\ & \left. + \bar{d}^L \gamma^\mu \left(-\frac{1}{2} + \frac{1}{3} \sin^2 \theta_w \right) d^L + \bar{d}^R \gamma^\mu \left(\frac{1}{3} \sin^2 \theta_w \right) d^R \right], \end{aligned} \quad (1.33)$$

$$J_{\text{em}}^\mu = -\bar{e} \gamma^\mu e + \frac{2}{3} \bar{u} \gamma^\mu u - \frac{1}{3} \bar{d} \gamma^\mu d. \quad (1.34)$$

The W boson correctly couples only to LH fermions. Moreover, while the charged and neutral currents contain a vectorial and axial part, the electromagnetic current couples to the photon field in a purely vectorial way.

1.1.3 Yukawa sector

The SM picture is now almost complete. What is still missing is a mass term for the charged fermions. In fact, a Dirac mass of the type $m\bar{\psi}\psi$, which was gauge invariant in QED, cannot be introduced by hand in the Lagrangian since a term $\bar{e}^L e^R$ would break the $SU(2)_L$ invariance. We write down a gauge invariant operator that couples LH and RH fermions to the Higgs field, such that the masses appear only after the SSB mechanism. Focusing now on the first generation only, it reads

$$\mathcal{L}_{\text{Yukawa}} = -y_e \bar{L}_j^L \phi e^R - y_d \bar{Q}^L \phi d^R - y_u \bar{Q}^L \tilde{\phi} u^R + \text{h.c.} \quad (1.35)$$

where $\tilde{\phi} = i\sigma^2 \phi^*$ and $y_{e,u,d}$ are the Yukawa couplings. When expanding this vertex in the unitary gauge, $\mathcal{L}_{\text{Yukawa}}$ takes the form

$$\mathcal{L}_{\text{Yukawa}} = - \sum_{f=e,u,d} \left(m_f \bar{\psi}_f \psi_f + \frac{y_f}{\sqrt{2}} \bar{\psi}_f \psi_f h \right) \quad (1.36)$$

thus providing fermions with a mass

$$m_f = \frac{y_f v}{\sqrt{2}}. \quad (1.37)$$

The CKM matrix

When we introduce additional generations of quarks, there are additional coupling terms that mix generations:

$$\mathcal{L}_{\text{Yukawa}}^q = - \sum_{i,j} \left(y_d^{ij} \bar{Q}_i^L \phi d_j^R + y_u^{ij} \bar{Q}_i^L \tilde{\phi} u_j^R \right) + \text{h.c.} \quad (1.38)$$

having introduced $u_i = (u, c, t)$ and $d_i = (d, s, b)$. After EWSB the mass terms become

$$\mathcal{L}_{\text{Yukawa}}^{q,\text{masses}} = - \frac{v}{\sqrt{2}} \left(\bar{d}^L \mathbb{Y}_d d^R + \bar{u}^L \mathbb{Y}_u u^R \right) + \text{h.c.} \quad (1.39)$$

The matrices of Yukawa couplings $\mathbb{Y}_{u,d}$ can be diagonalised with a biunitary transformation

$$\mathbb{Y}_d = U_d^L \mathbb{D}_d U_d^{R\dagger}, \quad \mathbb{Y}_u = U_u^L \mathbb{D}_u U_u^{R\dagger} \quad (1.40)$$

that transform the fields into the mass basis d', u' :

$$d^{L,R} = U_d^{L,R} d'^{L,R'}, \quad u^{L,R} = U_u^{L,R} u'^{L,R'}. \quad (1.41)$$

When we rotate the fields in the new basis, the fermionic part of the Lagrangian is affected too. In particular, the neutral current J_Z^μ does not mix up-like and down-like components and therefore remains flavor conserving. On the other hand, the charged current $J_W^{\mu\pm}$ is transformed:

$$J_W^{\mu+} = \frac{1}{\sqrt{2}} \bar{u}^L \gamma^\mu d^L = \frac{1}{\sqrt{2}} \bar{u}^{L'} \gamma^\mu (U_u^{L\dagger} U_d^L) d^{L'}. \quad (1.42)$$

The mixing matrix $V \equiv U_u^\dagger U_d$ is called Cabibbo-Kobayashi-Maskawa (CKM) matrix. It is unitary, being the product of unitary matrices, and as a complex 3×3 matrix it depends on 9 real parameters, 3 angles and 6 phases. Actually, 5 of the 6 phases can be reabsorbed into the the fields, so the physical parameters are only 3 angles and 1 phase.

1.2 Unitarity cancellations in the SM

A very powerful application that follows from the SSB mechanism is the influence of the Higgs field on the high-energy dynamics of the vector bosons W^\pm and Z . Indeed, the unphysical Goldstone boson that is eaten by a massive gauge boson leaves a footprint in the high-energy limit of physical observables, by controlling the amplitude for absorption and emission of the gauge boson in its longitudinal polarization state. This result is formalised in the Goldstone Boson Equivalence (GBE) theorem [5], which has a fundamental application in the proof of the unitarity of the SM amplitudes [6].

1.2.1 Goldstone Boson Equivalence theorem

In the SSB mechanism, a massless gauge boson becomes massive by combining with a scalar Goldstone boson. This increases its polarization states from 2 to 3.

In its rest frame with $p^\mu = (m, 0, 0, 0)$, the 3 polarization are given by a basis of three orthogonal vectors satisfying $\epsilon_\mu p^\mu = 0$ and $\epsilon^2 = -1$:

$$\epsilon_+ = \frac{1}{\sqrt{2}} \begin{pmatrix} 0 \\ 1 \\ i \\ 0 \end{pmatrix}, \quad \epsilon_- = \frac{1}{\sqrt{2}} \begin{pmatrix} 0 \\ 1 \\ -i \\ 0 \end{pmatrix}, \quad \epsilon_L = \begin{pmatrix} 0 \\ 0 \\ 0 \\ 1 \end{pmatrix}. \quad (1.43)$$

These states are completely equivalent, but when the particle is moving relativistically, there is a clear distinction between the transverse and longitudinal polarizations [7]. If we make a boost along the z -axis, the momentum is $p^\mu = (E, 0, 0, p)$ and the polarization vectors become

$$\epsilon_+ = \frac{1}{\sqrt{2}} \begin{pmatrix} 0 \\ 1 \\ i \\ 0 \end{pmatrix}, \quad \epsilon_- = \frac{1}{\sqrt{2}} \begin{pmatrix} 0 \\ 1 \\ -i \\ 0 \end{pmatrix}, \quad \epsilon_L = \frac{1}{m} \begin{pmatrix} p \\ 0 \\ 0 \\ E \end{pmatrix}. \quad (1.44)$$

The transverse polarizations ϵ_+, ϵ_- are left unchanged, but for the longitudinal polarization ϵ_L the components are growing with energy. A distinctive feature is that it becomes increasingly parallel to p^μ as p grows. In fact

$$\epsilon_L^\mu = \frac{p^\mu}{m} + \mathcal{O}\left(\frac{m}{E}\right) \quad \text{as } E \rightarrow \infty. \quad (1.45)$$

This potentially leads to very large contributions to scattering amplitudes of longitudinally polarized vector bosons for $E \gg m$, threatening unitarity. The reason why this does not happen is in the GBE theorem by Cornwall, Levin, and Tiktopoulos and Vayonakis [5].

When a gauge boson acquires mass via Higgs mechanism, it “steals” a degree of freedom from the Higgs field, namely a scalar Goldstone boson. When the boson is highly boosted, the origin of the new longitudinal polarization becomes manifest.

According to the GBE theorem, in the high-energy limit, the couplings of the longitudinal polarization state are the same of the original Goldstone boson, so for example, considering a Z^0 boson

$$\mathcal{M}(X \rightarrow Y + Z_L^0) = i\mathcal{M}(X \rightarrow Y + G_z) \left(1 + \mathcal{O}\left(\frac{m_Z}{E_Z}\right)\right). \quad (1.46)$$

Since the scalar cross sections behave as $1/s$, some cancellations must happen between longitudinally polarized amplitudes that preserve this behavior.

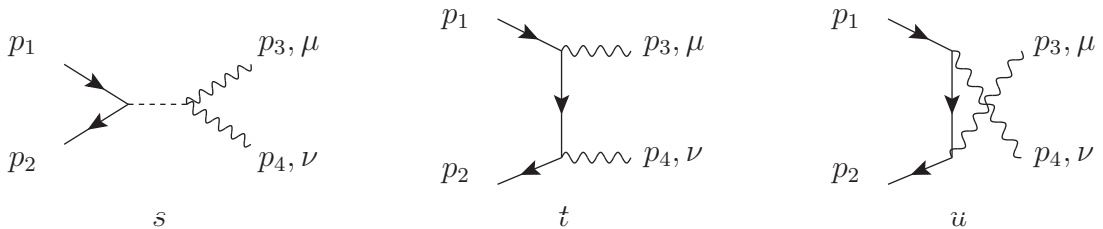
1.2.2 High-energy behavior in $\mu^+\mu^- \rightarrow ZZ$

As an example of unitarity cancellations happening in the SM, we consider the process $\mu^+\mu^- \rightarrow ZZ$ and show that

- the energy enhancement is due to the longitudinal polarizations,
- the Higgs field cancels the dangerous terms, preserving unitarity.

Kinematics

There are three diagrams, an s , a t and a u channel:



Suppose Z is boosted along the z -axis, its momentum is given by $p^\mu = (E_Z, 0, 0, p)$ and the polarization vectors are given by eqs. (1.44). Since we are interested in the high-energy limit of the longitudinal polarizations, we are going to use the approximation in eq. (1.45).

For spinors, we use the Dirac basis of gamma matrices:

$$\gamma^0 = \begin{pmatrix} 1 & 0 \\ 0 & -1 \end{pmatrix}, \quad \gamma^i = \begin{pmatrix} 0 & \sigma^i \\ -\sigma^i & 0 \end{pmatrix}, \quad \gamma^5 = \begin{pmatrix} 0 & 1 \\ 1 & 0 \end{pmatrix}. \quad (1.47)$$

We introduce a basis for the 2-components spinors, ξ^r and η^r , $r = +, -$ such that

$$\xi^{r\dagger} \xi^s = \delta^{rs}, \quad \eta^{r\dagger} \eta^s = \delta^{rs}, \quad (1.48)$$

for example

$$\left\{ \xi^+ = \begin{pmatrix} 1 \\ 0 \end{pmatrix}, \xi^- = \begin{pmatrix} 0 \\ 1 \end{pmatrix} \right\} \quad \text{and} \quad \left\{ \eta^+ = \begin{pmatrix} 1 \\ 0 \end{pmatrix}, \eta^- = \begin{pmatrix} 0 \\ 1 \end{pmatrix} \right\}. \quad (1.49)$$

Using the Dirac basis, the four solutions of Dirac equations are:

$$u_\pm(p_1) = \begin{pmatrix} \sqrt{E_1 + m_\mu} \xi_\pm \\ \frac{\vec{p}_1 \cdot \vec{\sigma}}{\sqrt{E_1 + m_\mu}} \xi_\pm \end{pmatrix}, \quad v_\pm(p_2) = \begin{pmatrix} \frac{\vec{p}_2 \cdot \vec{\sigma}}{\sqrt{E_2 + m_\mu}} \eta_\pm \\ \sqrt{E_2 + m_\mu} \eta_\pm \end{pmatrix} \quad (1.50)$$

where $\vec{\sigma} = (\sigma^1, \sigma^2, \sigma^3)$ and $p_i^\mu = (E_i, \vec{p}_i)$, $p_i^2 = m_\mu^2$, $i = 1, 2$.

In the CM frame the initial momenta are directed along the z axis, therefore

$$p_1 = (E, 0, 0, p), \quad p_2 = (E, 0, 0, -p) \quad (1.51)$$

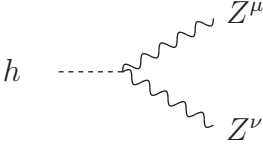
and the spinors are just

$$u_\pm(p_1) = \begin{pmatrix} \sqrt{E + m_\mu} \xi_\pm \\ \frac{p \sigma^3}{\sqrt{E + m_\mu}} \xi_\pm \end{pmatrix}, \quad v_\pm(p_2) = \begin{pmatrix} \frac{-p \sigma^3}{\sqrt{E + m_\mu}} \eta_\pm \\ \sqrt{E + m_\mu} \eta_\pm \end{pmatrix}. \quad (1.52)$$

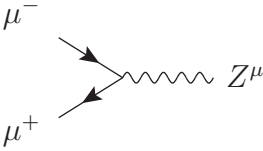
Feynman rules

In order to compute the matrix elements associated to the three diagrams we need the following Feynman rules:

$$\begin{array}{c} \mu^- \\ \nearrow \\ \mu^+ \nearrow \end{array} \text{---} h = -i \frac{y_\mu}{\sqrt{2}} = -i \frac{m_\mu}{v}, \quad (1.53)$$



$$h \text{ --- } \begin{array}{l} \text{wavy } Z^\mu \\ \text{wavy } Z^\nu \end{array} = i \frac{g_2}{c_w} m_Z g^{\mu\nu}, \quad (1.54)$$



$$\begin{array}{l} \mu^- \\ \mu^+ \end{array} \text{ --- } \text{wavy } Z^\mu = -i \frac{g_2}{c_w} \gamma^\mu (g_V - g_A \gamma^5), \quad (1.55)$$

where v is the vacuum expectation value of the Higgs field, y_μ is the Yukawa coupling of the muon, g_2 is the electroweak coupling of $SU(2)_L$, $c_w = \cos \theta_w$, $s_w = \sin \theta_w$ and θ_w is the Weinberg angle.

The electroweak masses and couplings are related by the following equations:

$$\begin{aligned} g &= \frac{e}{s_w}, & G_F &= \frac{1}{\sqrt{2} v^2}, \\ m_Z &= \frac{m_W}{c_w}, & m_W &= \frac{g_2 v}{2}, & m_\mu &= \frac{y_\mu v}{\sqrt{2}}. \end{aligned} \quad (1.56)$$

The vector and axial part of the vertex in eq. (1.55) are:

$$g_V = \frac{I_\mu^3}{2} - Q_\mu s_w^2 = \frac{1}{4} + s_w^2, \quad g_A = \frac{I_\mu^3}{2} = \frac{1}{4}, \quad (1.57)$$

where I_μ^3 and Q_μ are the third component of the weak isospin and the $U(1)_{\text{em}}$ charge of the muon.

Matrix elements in the high-energy limit

We start from the s channel amplitude, using the approximation for longitudinal polarizations in eq. (1.45).

$$\begin{aligned} i\mathcal{M}_s &= \bar{v}(p_2) \left(-i \frac{y_\mu}{\sqrt{2}} \right) u(p_1) \frac{i}{s - m_h^2} \epsilon^{\mu*}(p_3) \epsilon^{\nu*}(p_4) \frac{i g}{c_w} m_Z g_{\mu\nu} \\ &= i \frac{m_\mu}{v} \frac{g m_Z}{c_w} \frac{1}{s - m_h^2} \bar{v}(p_2) u(p_1) \epsilon^*(p_3) \cdot \epsilon^*(p_4). \end{aligned} \quad (1.58)$$

For $E \gg m_Z$:

$$\epsilon^*(p_3) \cdot \epsilon^*(p_4) \sim \frac{p_3 \cdot p_4}{m_Z^2} = \frac{1}{2} \frac{s - 2m_Z^2}{m_Z^2} \sim \frac{s}{2m_Z^2} \quad (1.59)$$

so that the amplitude in the high-energy limit is:

$$\mathcal{M}_s \sim \frac{m_\mu}{v} \frac{g m_Z}{c_w} \frac{1}{s} \frac{s}{2 m_Z^2} \bar{v}(p_2) u(p_1) = \frac{m_\mu}{v} \frac{g}{2 c_w m_Z} \bar{v}(p_2) u(p_1). \quad (1.60)$$

We work out the spinor product in the Dirac basis using eqs. (1.52):

$$\begin{aligned} \bar{v}_r(p_2) u_s(p_1) &= v_r^\dagger(p_2) \gamma^0 u_s(p_1) \\ &= \left(\eta_r^\dagger \frac{-p \sigma^3}{\sqrt{E+m_\mu}} \quad \eta_r^\dagger \sqrt{E+m_\mu} \right) \begin{pmatrix} 1 & 0 \\ 0 & -1 \end{pmatrix} \begin{pmatrix} \sqrt{E+m_\mu} \xi_s \\ \frac{p \sigma^3}{\sqrt{E+m_\mu}} \xi_s \end{pmatrix} \\ &= -2 p \eta_r^\dagger \sigma^3 \xi_s \sim -2 E \eta_r^\dagger \sigma^3 \xi_s = -\sqrt{s} \eta_r^\dagger \sigma^3 \xi_s. \end{aligned} \quad (1.61)$$

Using the definition of the 2-components spinors in eqs. (1.49):

$$\begin{aligned} \sigma^3 \xi_+ &= \xi_+, & \sigma^3 \eta_+ &= \eta_+, \\ \sigma^3 \xi_- &= -\xi_-, & \sigma^3 \eta_- &= -\eta_-. \end{aligned} \quad (1.62)$$

Therefore, if the spinors are in the same helicity state:

$$\bar{v}_+(p_2) u_+(p_1) = -\sqrt{s}, \quad \bar{v}_-(p_2) u_-(p_1) = \sqrt{s}, \quad (1.63)$$

while if they are in opposite helicity states the product is identically 0:

$$\bar{v}_+(p_2) u_-(p_1) = \bar{v}_-(p_2) u_+(p_1) = 0. \quad (1.64)$$

Finally, the polarized matrix element for the s channel is

$$\mathcal{M}_s(\mu_R^+ \mu_L^- \rightarrow Z_L Z_L) = \mathcal{M}_s(\mu_L^+ \mu_R^- \rightarrow Z_L Z_L) = 0 \quad (1.65)$$

for opposite polarizations, while for muon in the same polarization state it is

$$\begin{aligned} \mathcal{M}_s(\mu_{R,L}^+ \mu_{R,L}^- \rightarrow Z_L Z_L) &\xrightarrow{E \gg m_Z} \frac{m_\mu}{v} \frac{g}{2 m_W} \bar{v}_\pm(p_2) u_\pm(p_1) = \\ &\frac{m_\mu}{4 v^2} (\mp \sqrt{s}) = \mp \sqrt{2} G_F m_\mu \sqrt{s}. \end{aligned} \quad (1.66)$$

Here, the indices R and L stand for the positive and negative helicities respectively.

Now we look at the t and u channels. Starting from t

$$\begin{aligned} i \mathcal{M}_t &= \bar{v}(p_2) \left(-i \frac{g}{c_w} \right) \gamma^\mu (g_V - g_A \gamma^5) \epsilon_\mu^*(p_4) \frac{i(\not{p}_1 - \not{p}_3 + m_\mu)}{t - m_\mu^2} \\ &\quad \cdot \left(-i \frac{g}{c_w} \right) \gamma^\nu (g_V - g_A \gamma^5) \epsilon_\nu^*(p_3) u(p_1) \\ &\sim -i \left(\frac{g}{c_w} \right)^2 \bar{v}(p_2) \frac{\not{p}_4}{m_Z} (g_V - g_A \gamma^5) \frac{\not{p}_1 - \not{p}_3 + m_\mu}{t - m_\mu^2} \frac{\not{p}_3}{m_Z} (g_V - g_A \gamma^5) u(p_1) \\ &= -i \left(\frac{g}{c_w m_Z} \right)^2 \frac{1}{t - m_\mu^2} [\bar{v}(p_2) \not{p}_4 (g_V - g_A \gamma^5)^2 (\not{p}_1 - \not{p}_3) \not{p}_3 u(p_1) + \\ &\quad + m_\mu \bar{v}(p_2) \not{p}_4 (g_V - g_A \gamma^5) (g_V + g_A \gamma^5) (\not{p}_1 - \not{p}_3) \not{p}_3 u(p_1)] \end{aligned} \quad (1.67)$$

we get, after some algebra,

$$\mathcal{M}_t = - \left(\frac{g}{c_w m_Z} \right)^2 \frac{1}{t - m_\mu^2} (V + A) \quad (1.68)$$

where the vector and axial part are

$$V = (g_V^2 + g_A^2) (m_\mu^2 - t) \bar{v}(p_2) \not{p}_4 u(p_1) - 2 g_A^2 m_\mu \bar{v}(p_2) \not{p}_4 \not{p}_3 u(p_1), \quad (1.69)$$

$$A = 2 g_V g_A (m_\mu^2 - t) \bar{v}(p_2) \not{p}_4 \gamma^5 u(p_1) + 2 g_V g_A m_\mu \bar{v}(p_2) \not{p}_4 \gamma^5 \not{p}_3 u(p_1). \quad (1.70)$$

Using gamma algebra and the Dirac equation to simplify these expressions, we get

$$\begin{aligned} V + A &= (t - m_\mu^2) \bar{v}(p_2) \not{p}_4 \left[- (g_V^2 + g_A^2) + 2 g_V g_A \gamma^5 \right] u(p_1) \\ &\quad - 4 g_A^2 m_\mu^2 \bar{v}(p_2) \not{p}_4 u(p_1) + (t - m_\mu^2) m_\mu \left[2 g_A^2 + 2 g_V g_A \gamma^5 \right] u(p_1) \end{aligned} \quad (1.71)$$

and finally

$$\begin{aligned} \mathcal{M}_t &= - \left(\frac{g}{m_W} \right)^2 \frac{1}{t - m_\mu^2} \left[-4 g_A^2 m_\mu^2 \bar{v}(p_2) \not{p}_4 u(p_1) \right] \\ &\quad - \left(\frac{g}{m_W} \right)^2 \bar{v}(p_2) \not{p}_4 \left[- (g_V^2 + g_A^2) + \bar{v}(p_2) 2 g_V g_A \gamma^5 \right] u(p_1) \\ &\quad - \left(\frac{g}{m_W} \right)^2 \bar{v}(p_2) m_\mu \left(2 g_A^2 + 2 g_V g_A \gamma^5 \right) u(p_1). \end{aligned} \quad (1.72)$$

Similarly, for the u channel:

$$\begin{aligned} \mathcal{M}_u &= - \left(\frac{g}{m_W} \right)^2 \frac{1}{u - m_\mu^2} \left[-4 g_A^2 m_\mu^2 \bar{v}(p_2) \not{p}_3 u(p_1) \right] \\ &\quad - \left(\frac{g}{m_W} \right)^2 \bar{v}(p_2) \not{p}_3 \left[- (g_V^2 + g_A^2) + \bar{v}(p_2) 2 g_V g_A \gamma^5 \right] u(p_1) \\ &\quad - \left(\frac{g}{m_W} \right)^2 \bar{v}(p_2) m_\mu \left(2 g_A^2 + 2 g_V g_A \gamma^5 \right) u(p_1). \end{aligned} \quad (1.73)$$

Combining the two amplitudes, the axial part cancels leaving only the vectorial and scalar ones:

$$\begin{aligned} \mathcal{M}_t + \mathcal{M}_u &= \frac{g^2}{m_W^2} 4 m_\mu^2 g_A^2 \bar{v}(p_2) \left(\frac{\not{p}_4}{t - m_\mu^2} + \frac{\not{p}_3}{u - m_\mu^2} \right) u(p_1) \\ &\quad - \frac{g^2}{m_W^2} 4 m_\mu g_A^2 \bar{v}(p_2) u(p_1). \end{aligned} \quad (1.74)$$

In the high-energy limit we can neglect masses in the denominators of the propagators and approximate the Mandelstam variables as

$$t \sim u \sim -\frac{s}{2} \quad (1.75)$$

so that

$$\mathcal{M}_t + \mathcal{M}_u \xrightarrow{E \gg m_Z} -\frac{g^2}{m_W^2} 4 m_\mu g_A^2 \bar{v}(p_2) u(p_1) = -\frac{g^2}{4 m_W^2} m_\mu \bar{v}(p_2) u(p_1). \quad (1.76)$$

Finally, the polarized matrix elements for the t and u channels are:

$$\begin{aligned} \mathcal{M}_{t+u}(\mu_R^+ \mu_L^- \rightarrow Z_L Z_L) & \xrightarrow{E \gg m_Z} 0, \\ \mathcal{M}_{t+u}(\mu_L^+ \mu_R^- \rightarrow Z_L Z_L) & \end{aligned} \quad (1.77)$$

$$\begin{aligned} \mathcal{M}_{t+u}(\mu_R^+ \mu_R^- \rightarrow Z_L Z_L) & \xrightarrow{E \gg m_Z} -\frac{g^2}{4 m_W^2} m_\mu (\mp \sqrt{s}) = \pm \sqrt{2} G_F m_\mu \sqrt{s}. \\ \mathcal{M}_{t+u}(\mu_L^+ \mu_L^- \rightarrow Z_L Z_L) & \end{aligned} \quad (1.78)$$

To sum up, the longitudinal polarizations of the vectors are responsible for the potential energy growth of the matrix element, however for muons in opposite polarization states the s channel is identically 0, and the $t + u$ channels are suppressed independently with growing \sqrt{s} :

$$\mathcal{M}_{s+t+u}(\mu_R^+ \mu_L^- \rightarrow Z_L Z_L), \mathcal{M}_{s+t+u}(\mu_L^+ \mu_R^- \rightarrow Z_L Z_L) \xrightarrow{E \gg m_Z} 0. \quad (1.79)$$

For muons in the same polarization state, the t and u channels have a dependence on \sqrt{s} , but this is exactly cancelled by the diagram with the Higgs:

$$\begin{aligned} \mathcal{M}_{s+t+u}(\mu_R^+ \mu_R^- \rightarrow Z_L Z_L) & \xrightarrow{E \gg m_Z} \mp \sqrt{2} G_F m_\mu \sqrt{s} \pm \sqrt{2} G_F m_\mu \sqrt{s} = 0. \\ \mathcal{M}_{s+t+u}(\mu_L^+ \mu_L^- \rightarrow Z_L Z_L) & \end{aligned} \quad (1.80)$$

This last cancellation among the s and the $t + u$ channels is particularly surprising, since the first diagram depends on the Higgs couplings, while the other two are not in any way related to the presence of the Higgs, at least apparently. Indeed the mass of the muon multiplying \sqrt{s} is provided by the Higgs mechanism, and the presence of the Higgs scalar is necessary to unitarize the SM by compensating for this growth in energy.

Chapter 2

Investigating the Higgs couplings

The first two runs of LHC have provided a decisive test of the SM, confirming the success of the present description of strong and electroweak interactions at present energies. In particular, an important milestone was set by the discovery in 2012 of a scalar boson fitting the properties of the SM Higgs, with a single doublet and the minimal set of interactions providing the fermions and gauge bosons masses, completing the particle content of the SM.

Up to now all the experimental results at colliders are compatible with SM predictions. However, while the gauge interactions have been probed with great precision, the tests of the Higgs boson interactions have not yet reached the same level of accuracy. The Higgs sector is therefore the most mysterious and less understood sector of the SM, and improving the precision on Higgs parameters is among the most pressing issues of any future program in particle physics.

2.1 Overview on Higgs couplings measurements

After the conclusion of LHC Run II in 2018, a major improvement on the measures of the Higgs properties is expected with the high luminosity LHC (HL-LHC) upgrade [8], [9]. Meanwhile, the discussion over which future collider will come next is already taking place.

2.1.1 Higgs interactions at LHC

The left panel of Figure 2.1 [10] presents the current relative precision on Higgs couplings measurements, and the projections for HL-LHC. Here and in what follows, the parameter κ_i , defined as

$$\kappa_i \equiv \frac{g_i}{g_i^{\text{SM}}} \tag{2.1}$$

specifies the deviation of the coupling g_i of the Higgs boson to a given particle i from the SM expectation. The couplings to gauge bosons can be measured through the diboson decays of the Higgs into $\gamma\gamma$, ZZ and WW , and their current uncertainty is around 10%. On the other hand, the Yukawa sector has not yet been tested at the same level of precision. On the right of Figure 2.1 are shown the 2021 results from the CMS experiment [3]. The best information currently available is on the Higgs couplings to the third-generation charged fermions, while the only evidence of the Yukawa coupling to the first two generations of fermions is the muon Yukawa coupling, which has an uncertainty of about 100%.

With the HL-LHC, significant improvements are expected for the Higgs couplings with gauge bosons, reaching a relative precision of 1 – 2%. Moreover, the muon coupling will be measured with an uncertainty of 4%.

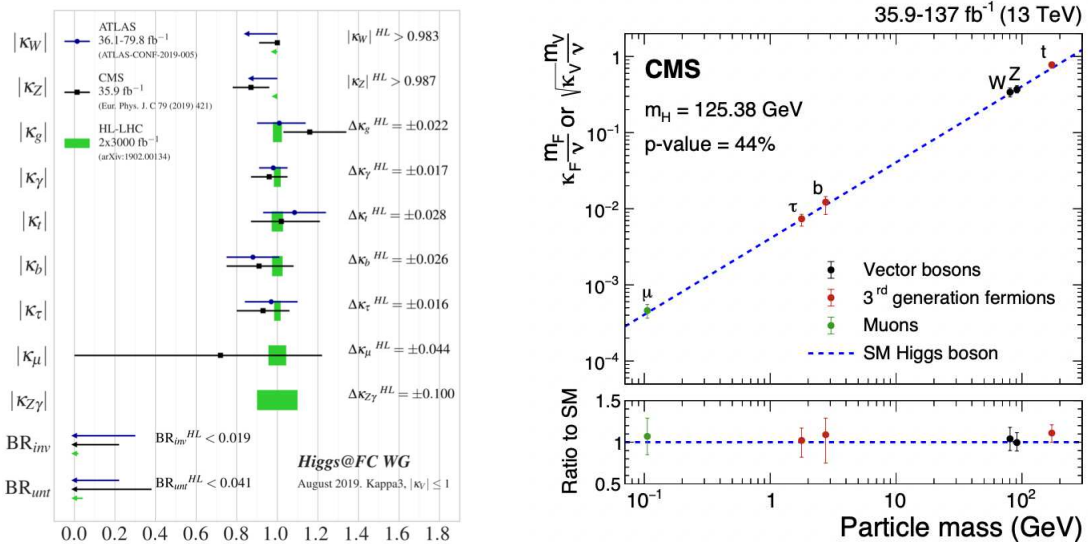


Figure 2.1: Left: relative precision on Higgs coupling modifiers κ_i , determined by ATLAS and CMS with the LHC data at present, and as expected for HL-LHC. Right: the best fit estimates for the Yukawa couplings at CMS compared to their corresponding prediction from the SM. In the lower panel, the ratios of the measured coupling modifiers values to their SM predictions are shown.

2.1.2 Future perspectives

Different types of future colliders are being discussed, and their predicted uncertainties on the Higgs couplings are reported in Table 2.2, combined with HL-LHC results [11]. One of the proposals for the next collider facility is an electron-positron collider running at the

kappa-3 scenario	HL-LHC+									
	ILC ₂₅₀	ILC ₅₀₀	ILC ₁₀₀₀	CLIC ₃₈₀	CLIC ₁₅₀₀	CLIC ₃₀₀₀	CEPC	FCC-ee ₂₄₀	FCC-ee ₃₆₅	FCC-ee/eh/hh
κ_W [%]	1.0	0.29	0.24	0.73	0.40	0.38	0.88	0.88	0.41	0.19
κ_Z [%]	0.29	0.22	0.23	0.44	0.40	0.39	0.18	0.20	0.17	0.16
κ_g [%]	1.4	0.85	0.63	1.5	1.1	0.86	1.	1.2	0.9	0.5
κ_γ [%]	1.4	1.2	1.1	1.4*	1.3	1.2	1.3	1.3	1.3	0.31
$\kappa_{Z\gamma}$ [%]	10.*	10.*	10.*	10.*	8.2	5.7	6.3	10.*	10.*	0.7
κ_c [%]	2.	1.2	0.9	4.1	1.9	1.4	2.	1.5	1.3	0.96
κ_s [%]	3.1	2.8	1.4	3.2	2.1	2.1	3.1	3.1	3.1	0.96
κ_b [%]	1.1	0.56	0.47	1.2	0.61	0.53	0.92	1.	0.64	0.48
κ_μ [%]	4.2	3.9	3.6	4.4*	4.1	3.5	3.9	4.	3.9	0.43
κ_τ [%]	1.1	0.64	0.54	1.4	1.0	0.82	0.91	0.94	0.66	0.46
BR _{inv} (<%, 95% CL)	0.26	0.23	0.22	0.63	0.62	0.62	0.27	0.22	0.19	0.024
BR _{unt} (<%, 95% CL)	1.8	1.4	1.4	2.7	2.4	2.4	1.1	1.2	1.	1.

Figure 2.2: Expected relative precision on Higgs coupling modifiers κ for future accelerators beyond the LHC era. An asterisk (*) indicates the cases in which the HL-LHC dominates the combination. FCC-ee/eh/hh corresponds to the combined performance of FCC-ee₂₄₀+FCC-ee₃₆₅, FCC-eh and FCC-hh.

Zh threshold energy (Higgs factory) [10], such as the International Linear Collider (ILC) [12],[13], the Future Circular Collider (FCC-ee)[14] or the Circular Electron-Positron Collider (CEPC) [15], while the Compact Linear Collider (CLIC) [16] would run in the multi-TeV range. Alternatively, lepton-hadron or hadron-hadron colliders like the FCC-eh and the FCC-hh are expected to reach respectively 50 and 100 TeV [17]. Compared to the HL-LHC, the e^+e^- colliders improve most parameters by about factors of 5-10, with the exceptions of top, γZ and μ couplings. For fermions, the best sensitivity is reached for b quarks and τ , and it is below 1%.

2.2 The muon Yukawa coupling

The next target in the investigation of Higgs properties is the muon Yukawa coupling. Reaching a better precision on this measure is interesting for several reasons.

On one hand the muon Yukawa is the most experimentally sensitive probe of the Higgs boson couplings to second-generation fermions at the LHC. Since the last results are not yet at the 5σ level for discovery, there is still room for $\mathcal{O}(100\%)$ corrections.

Moreover, some recent issues, like the anomalous muon $g - 2$ and the discrepancy between the branching ratios of B -meson decay to muons and electrons, are suggesting the presence of potential new physics related to muons, motivating a deeper investigation on muon properties.

Finally, among the many future accelerators proposals on the table, there is a high-energy muon collider, which holds interesting prospects for new physics searches at the energy frontier as well as precision measurements for SM physics and beyond, in particular in connection with the muon anomalies.

All these arguments are prompting the interest towards the study of processes that would allow a better sensitivity on this currently elusive parameter.

2.2.1 Muon anomalies

The recent $g - 2$ and B -decay anomalies offer experimental hints for flavour-violating new physics that point strongly and specifically to muons. If confirmed, these anomalies might become primary drivers for particle physics research, supporting the need for a deeper investigation on muon properties.

Muon $g - 2$

The magnetic and electric dipole moments are intrinsic properties of charged spinning particles like the leptons.

On the classical level, an orbiting particle with electric charge e and mass m has a magnetic dipole moment given by

$$\vec{\mu}_m = \frac{e}{2m} \vec{L} \quad (2.2)$$

where \vec{L} is the angular momentum, and an electrical dipole moment \vec{d}_e can be present due to a relative displacement between the centers of positive and negative charges. These moments contribute to the electromagnetic interaction Hamiltonian with electric and magnetic fields \vec{E} and \vec{B} as

$$\mathcal{H} = -\vec{\mu}_m \cdot \vec{B} - \vec{d}_e \cdot \vec{E} . \quad (2.3)$$

For a particle with spin, the magnetic moment is intrinsic and is obtained by replacing the angular momentum operator \vec{L} with the spin operator $\vec{S} = \vec{\sigma}/2$

$$\vec{\mu}_m = g Q \frac{e}{2m} \vec{S} \quad (2.4)$$

where g is called gyromagnetic factor. Dirac equation correctly predicts a value of $g = 2$ for a free electron (and in general an elementary fermion like the muon), twice the value $g = 1$ known to be associated with orbital angular momentum.

However, when QFT is taken into account, the $g - 2$ receives radiative corrections from perturbative loops in the $\mu^+ \mu^- \gamma$ interaction. The deviation from the Dirac (tree-level) result is the anomalous magnetic moment

$$a \equiv \frac{g - 2}{2} . \quad (2.5)$$

The anomalous magnetic moment of the electron a_e is employed to determine the value of the fine-structure constant α , due to the extreme experimental precision on its measurement. It is therefore used as an input parameter in the SM. On the other hand, because

of the high precision of its theoretical and experimental determinations, the muon a_μ has always been considered a powerful test on new physics and has been recently measured with high precision. The SM contributions to the muon anomaly include electromagnetic, strong, and weak interactions that arise from virtual effects involving photons, leptons, hadrons, and the W , Z and Higgs bosons. The theoretical SM predictions [18] found a value of

$$a_\mu^{\text{th}} = 116591810(43) \cdot 10^{-11}. \quad (2.6)$$

On the experimental level, the Brookhaven (BNL) collaboration found in 2006 a value larger than a_μ^{th} by 3.7 standard deviations (σ) [19]. More recently, the Fermilab (FNAL) experiment obtained a value exceeding that of the SM by 3.3 σ [20], in agreement with BNL result. The experimental average

$$a_\mu^{\text{exp}} = 116592061(41) \cdot 10^{-11} \quad (2.7)$$

increases the significance of the discrepancy between a_μ^{th} and a_μ^{exp} to 4.2 σ as shown in Figure 2.3 [20], motivating the development of SM extensions.

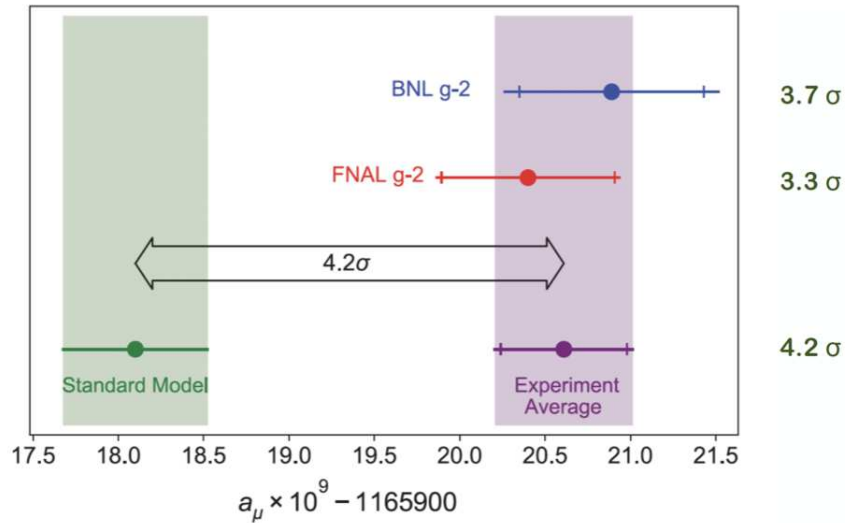


Figure 2.3: Experimental values of a_μ from BNL, FNAL, and the combined average. The SM prediction is also shown.

It is worth mentioning that lattice calculations for the hadronic contribution [21] predict a value compatible with experimental observations, and that further studies are being made on the topic.

***B*-meson decay anomaly**

A distinctive feature of the SM is that the different charged leptons, the electron, muon and tau, have identical electroweak interaction strengths. This principle is known as

lepton universality, and the only exception in the SM is the lepton-Higgs interaction, being dependent on the different lepton masses.

Previous measurements have shown a wide range of particle decays are consistent with this principle of lepton universality. However, in 2021 the LHCb experiment provided evidence for the breaking of lepton universality in beauty-quark decays, with a significance of 3.1 standard deviations. The measurements are of processes in which a beauty meson like B^+ transforms into a strange meson (K^+) with the emission of two charged leptons, either e^+e^- or $\mu^+\mu^-$. The B^+ hadron contains a beauty antiquark, \bar{b} , and the K^+ contains a strange antiquark, \bar{s} . Thus at the quark level the decay involves a $\bar{b} \rightarrow \bar{s}$ transition mediated in the SM by virtual γ , W^\pm , Z^0 bosons and the top quark, as shown in Figure 2.4 [22].

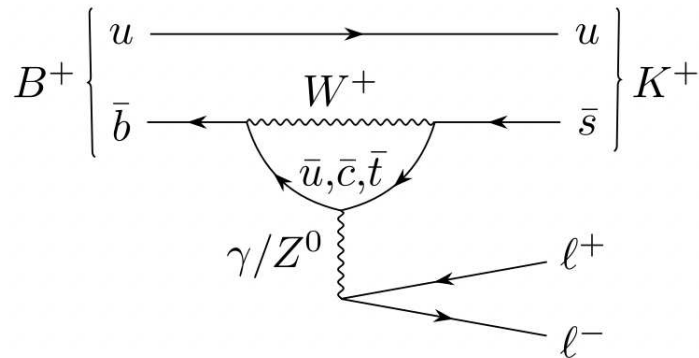


Figure 2.4: Fundamental processes contributing to $B^+ \rightarrow K^+ l^+ l^-$ decays in the SM.

The ratio between the branching fractions

$$R_K = \frac{\mathcal{B}(B^+ \rightarrow K^+ \mu^+ \mu^-)}{\mathcal{B}(B^+ \rightarrow K^+ e^+ e^-)} \quad (2.8)$$

is predicted with a precision of $\mathcal{O}(1\%)$ to be close to 1 [23–25], since the masses of electrons and muons are small compared to that of b and the difference is therefore negligible. Table 2.1 shows the recent measurements of the branching ratios at the LHCb experiment [22].

The ratio R_K was found to be 3.1σ below the SM expectation, giving evidence for the violation of lepton universality in this decay.

If confirmed by future measurements, this violation of lepton universality would imply physics beyond the Standard Model, such as a new fundamental interaction between quarks and leptons.

	LHCb-data '14,'21	SM
$\mathcal{B}(B^+ \rightarrow K^+ \mu^+ \mu^-)$	$(1.19 \pm 0.03 \pm 0.06) \cdot 10^{-7}$	$1.75 \cdot 10^{-7}$
$\mathcal{B}(B^+ \rightarrow K^+ e^+ e^-)$	$(1.40 \pm 0.07 \pm 0.06) \cdot 10^{-7}$	$1.75 \cdot 10^{-7}$
R_K	$0.846^{+0.044}_{-0.041}$	1.00 ± 0.01

Table 2.1: Branching ratios and their ratio R_K as measured at LHCb and their SM prediction.

2.2.2 Muon colliders

The high-energy muon collider is among the new accelerators that are being considered for the future advances in particle physics [26–30]. Despite their technological challenges, such facilities have great potential for precision measurements for SM physics and beyond, and for the investigations of muon properties in particular. Electron-positron and proton-proton colliders are typically associated with complementary strategies of exploration. While the former offer much more precise measurements, allowing for the search of indirect manifestation of new physics, the latter can access heavy particles directly thanks to a higher energy reach. Electrons are indeed subjected to a considerable energy loss due to the synchrotron radiation, which scales with the beam particle mass as $\sim m^{-4}$. Hence, because of the lightness of electrons, their energy reach is considerably limited, compared to protons. Muon colliders would combine the benefits of lepton and hadron colliders in a single machine that works effectively as a precision facility as well as an exploratory machine.

Muon colliders leverage the strength of leptonic colliders, which is they collide elementary particles. This means that:

- in first approximation their center-of-mass energy is known and it is entirely available for the hard scattering process, making leptonic collisions more effective than hadronic ones with comparable energy and luminosity,
- the final states are cleaner relative to those produced by the dissociation of composite particles, which instead generate a background of underlying events.

These advantages come at a cost. In fact there are severe technical challenges related to the fact that the muon is not stable, having a very short lifetime of $2.2 \mu\text{s}$. While the push to high momentum beams can extend the lab frame lifetime up to the order of seconds, the exponential decay of the muon produces an intense source of collinear off-momentum electrons. The electrons then interact with the beamline components, producing electromagnetic showers that result in a high flux of low-energy photons and soft neutrons; these are the primary source of background for a muon collider detector. Another important aspect must be taken into account: the decay neutrinos will produce a secondary radiation, with hadrons, muons and electrons traversing the earth that may constitute a radiological threat.

However, the technological development has already shown considerable progress in addressing these issues, making the muon collider a competitive candidate for high-energies future facilities.

Prospectives on Higgs couplings measurements

Two possible configurations of muon colliders have been proposed so far [26]: a muon collider running at the Higgs pole mass, and a higher energy collider operating in the multi-TeV range.

A 125 GeV muon collider could directly determine the Higgs width and couplings with a production channel $\mu^+\mu^- \rightarrow h$. The expected sensitivity reach is shown in Figure 2.5 [29], compared to that of HL-LHC and an e^+e^- collider at 240 GeV.

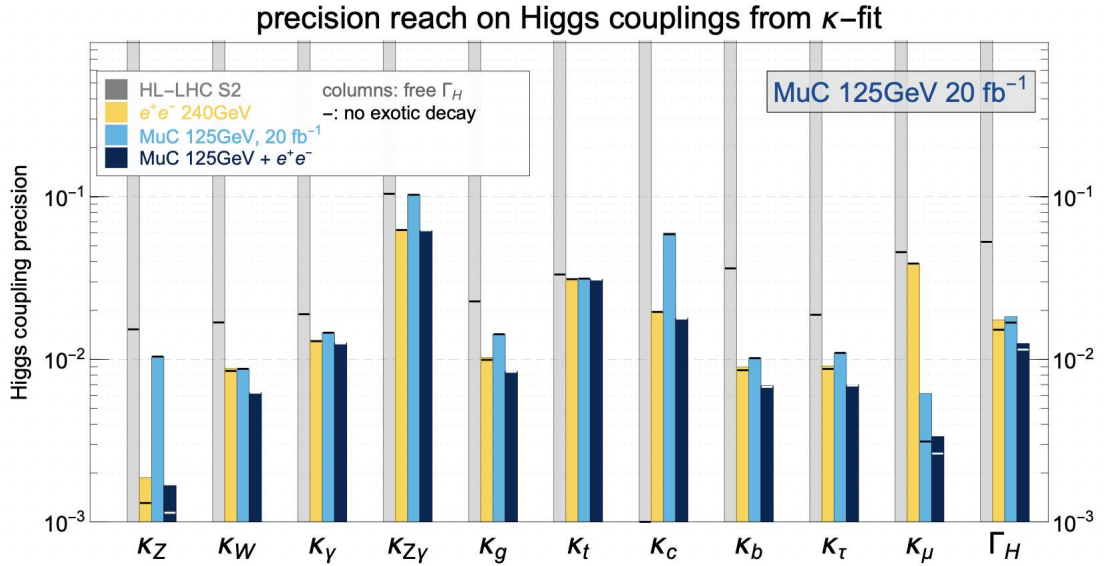


Figure 2.5: The Higgs couplings and decay width precisions at HL-LHC in the S2 scenario (which assumes that the current uncertainties can be reduced by a factor of two by the end of the HL-LHC), at a circular e^+e^- collider, at a 125 GeV muon collider, and the combination of e^+e^- and the muon collider. Lepton colliders scenarios are combined with the HL-LHC measurements. The column shows results with Γ_H treated as a free parameter, the horizontal marks show results assuming that the Higgs has no exotic decays.

Not surprisingly, the Higgs production channel gives the muon Yukawa coupling precision a significant boost of more than one order of magnitude, from $\sim 4\%$ to $\sim 0.4\%$, with which a future e^+e^- collider could not compete. On the other hand, a 240 GeV e^+e^- collider is much better at measuring the Higgs coupling to Z , thanks to its excellent

Zh production measurement. For the other couplings, the two colliders reaches are comparable when individually combined with HL-LHC.

Despite the considerable improvement on the measure of y_μ , the physics potential of a 125 GeV muon collider is not competitive with other colliders such as the Higgs factory. On the other hand, a multi-TeV muon collider would exploit the potential of muons in reaching extremely high energies, offering an indirect access to potential new physics with scale-dependent effects.

In what follows, motivated by the promising potential of a multi-TeV muon collider we lay the groundwork to determine its sensitivity in measuring the muon Yukawa coupling.

Chapter 3

Theoretical frameworks

Our goal is determining the precision on the measurement of the muon Yukawa. In order to compute new physics deviations from the SM, we need a framework to parametrize these effects. In the first section, we discuss two approaches, the Standard Model Effective Field Theory and the κ formalism. Then, we focus on the parametrization of muon-Higgs coupling deviations specifically and discuss some differences in the two approaches.

3.1 The SMEFT and κ formalisms

In the following we discuss two different parametrizations of new physics effects. The EFT framework is a well-defined Quantum Field Theory, allowing to perform consistently calculations below a certain energy scale and to make predictions on the heavier physics. On the other hand, experimental results are usually presented in the simpler κ framework, which however presents several deficiencies.

3.1.1 The Effective Field Theory approach

Effective theories are the low-energy limit of more fundamental theories. They allow to make meaningful predictions in situations characterized by sufficiently low energy scales, even when the exact theory is not known. This is not an exotic concept in physics. For example Newtonian mechanics provides a complete framework for the description of macroscopic and non-relativistic physics, even if the short distance properties of Nature are not known.

Just like any QFT, an Effective Field Theory (EFT) is a consistent theory that allows to compute measurable quantities without any additional input from the underlying theory. Calculations come with a finite error that depends on a small expansion parameter δ , the power counting. When the power n of the expansion is fixed, the error is of order

δ^{n+1} . The number of free parameters of the EFT Lagrangian depends on n and increases with increasing n [31].

Two different approaches to effective theories are possible, depending on whether the dynamics at high energy is known and calculable. If the full UV theory is known, we can work in a simpler context by integrating out the heavy physics. The resulting EFT has an infinite tower of local operators that are suppressed by powers of the heavy scale. If the full theory is not known, EFTs provide a parameterization of the unknown interactions, allowing to estimate their magnitudes and to classify their relative importance. The new operators can then be constrained with experimental data.

The reason why EFTs are applicable to both cases with the known and with the unknown high-energy theory is that in an effective description only the relevant degrees of freedom are used and the high-energy physics is encoded indirectly through interactions among the light states.

The decoupling theorem

The key principle of the effective theory is a separation of scales, summarised in the Appelquist-Carazzone decoupling theorem [32]. It states that, for a renormalizable unbroken gauge theory where different mass scales are present, at momenta small compared to the larger masses the dynamics is determined by the light sector of the theory. The role of the heavy fields in diagrams where they only appear as internal propagators is in their contribution to the coupling constant and the field strength renormalization.

These fields are removed from the theory by integrating them out of the original Lagrangian, producing the effective Lagrangian that can be used to compute low energy observables. This is formally done by performing a path integral over the heavy states ϕ_H only, so that the resulting Lagrangian depends only on the light fields ϕ_L [33]:

$$\int D\phi_H e^{i \int \mathcal{L}(\phi_L, \phi_H)} = e^{i \int \mathcal{L}_{\text{EFT}}(\phi_L)}. \quad (3.1)$$

The effective Lagrangian can be expanded into a series of local operators $\mathcal{O}_i^{(d)}$, where d is their mass dimension. The information on heavy degrees of freedom is encoded in the Wilson coefficients c_i :

$$\mathcal{L}_{\text{EFT}} = \sum_i \frac{c_i}{\Lambda^{d-4}} \mathcal{O}_i^{(d)}. \quad (3.2)$$

The effective theory is consistent when it is applied to processes at energies lower than Λ , which is the high-energy cutoff of the EFT. For these processes, the behavior of the operators is determined by their dimension, which classify them into three categories [34]:

- relevant ($d < 4$)
- marginal ($d = 4$)

- irrelevant ($d > 4$)

and their contribution to a matrix element is suppressed by a factor

$$\left(\frac{E}{\Lambda}\right)^{d-4}.$$

Irrelevant operators are thus small at low energies, while couplings of positive mass dimension give rise to effects which become large at energies much smaller than Λ and are called relevant. In 4 dimensions, the only possible relevant operators are

- $d = 0$: the unit operator,
- $d = 2$: boson mass term,
- $d = 3$: fermion mass term and cubic scalar interaction.

Marginal operators are equally important at all energy scales, and quantum effects could modify their scaling either toward the relevant or irrelevant side. Some examples are the ϕ^4 theory, QED, QCD and Yukawa interactions.

When there is a large gap between the scale E of the process and the heavy states, the irrelevant operators can be neglected and the resulting theory contains only relevant and marginal operators and is called renormalizable.

The SM as an EFT

The presence of Landau poles in the $SU(2)_L \times U(1)_Y$ theory suggests that the electroweak SM is an EFT valid up to a certain UV scale Λ . The more fundamental theory completing the picture is expected to involve some new particles heavier than the Higgs vev, which is the characteristic scale of the SM. A suitable UV completion should satisfy the following requirements [35]:

- it should contain the gauge group $SU(3)_C \times SU(2)_L \times U(1)_Y$,
- all the SM states should be included either as fundamental or composite fields,
- at energies $E < \Lambda$, it should match the SM up to corrections of order $\mathcal{O}(E/\Lambda)$.

According to the decoupling theorem, the heavy states leave some footprints in the low energy Lagrangian in the form of gauge invariant irrelevant operators.

The power of EFT description is that, even if the underlying theory is not known, it is possible to build an effective, model-independent Lagrangian describing the low-energy limit of a wide class of SM extensions. In the SM Effective Field Theory (SMEFT) the

new physics is parametrized by adding to the SM Lagrangian all possible local, higher-dimensional operators built out of the SM fields and preserving the fundamental gauge symmetry $SU(3)_C \times SU(2)_L \times U(1)_Y$:

$$\mathcal{L}_{\text{SMEFT}} = \mathcal{L}_{\text{SM}}^{(4)} + \frac{1}{\Lambda} \sum_i c_i^{(5)} \mathcal{O}_i^{(5)} + \frac{1}{\Lambda^2} \sum_i c_i^{(6)} \mathcal{O}_i^{(6)} + \dots \quad (3.3)$$

Their contribution is automatically ordered by the power expansion in $1/\Lambda$. This is in principle an infinite sum. In practice, just a few terms are relevant. Only a finite number of terms has to be kept because the theory needs to reproduce experiments to finite accuracy and also because the theory can be tailored to specific processes of interest. The higher the dimension of an operator, the smaller its contribution to low-energy observables. Hence, obtaining results to a given accuracy requires a finite number of terms.

The lowest dimension new term in the SMEFT is the only dimension 5 operator:

$$\mathcal{L}^{(5)} = \frac{c_{rs}^{(5)}}{\Lambda} \epsilon^{ij} \epsilon^{kl} (L_{ir}^T C L_{ks}) \phi_j \phi_l + \text{h.c.} \quad (3.4)$$

where r, s are flavor indices, i, j, k, l are $SU(2)_L$ indices and $C = i\gamma^2$ is the charge-conjugation operator. However, this term violates lepton number by 2 units. Therefore it is not present if we assume lepton number conservation. In this case, the most relevant effective operators are those of dimension 6. In absence of additional symmetries, the number of independent operators for each generation of fermions is 59, and 2499 for three generations. It is then reasonable to consider only a subset of operators when we study the sensitivity of a measurement.

Once the framework is set by introducing specific higher-dimensional operators, the measurements can be used to put constraints on the effective coefficients, from which we can extrapolate bounds on the UV theory.

3.1.2 The κ framework

The SMEFT is a well-defined QFT built with precise requirements that ensure consistency with the UV extensions of the SM. On the other hand, the formalism currently used to present experimental results is the κ framework, which we have already encountered in chapter 2. This approach is an ad-hoc rescaling of couplings in the SM without a field theory embedding, although a mapping can be performed when further UV assumptions are made. We summarise the main limitations of the κ framework with respect to the EFT.

- Since the complete theory can introduce new structures that are not captured by the κ framework, it is not always possible to map consistently the deviations from the κ fits to a UV quantum field theory.

- The κ formalism is not systematically improvable with perturbative corrections. The only way to determine perturbative corrections without assuming the SM is with an effective field theory embedding. Higher order calculations are however made necessary by the increasing experimental accuracy.
- The formulation is intrinsically non-gauge invariant. Since the couplings to the Higgs are left arbitrary, it will likely lead to non-unitary matrix elements. This is not a concern in an EFT, since it must be unitary only below the UV cutoff Λ . However, the κ formalism do not contain any cutoff scale in its definition that defines its range of validity and it is in principle consistent at all energies. For this reason, when it is not embedded in an EFT the violation of unitarity is problematic.

The κ framework was constructed as a first probe of the Higgs boson properties and constitutes a reasonable framework for testing the consistency of the experimental data with the SM Higgs. However, with the increased experimental precision, it is not an appropriate tool for a consistent analysis of the Higgs properties. An EFT description is more suited for future high-precision studies as it would overcome the main limitations of the κ framework.

3.2 Muon Yukawa coupling in SMEFT

Our target is the muon Yukawa coupling, so we consider a 6 dimensional operator affecting the muon coupling to the Higgs doublet

$$\mathcal{L}^{(6)} = \frac{c_6}{\Lambda^2} (\phi^\dagger \phi - \frac{v^2}{2}) (\bar{L} \phi_{\mu R} + \text{h.c.}). \quad (3.5)$$

The quantities entering eq. (3.5) are defined as follows:

$$\begin{aligned} \phi &= \begin{pmatrix} \phi^+ \\ \phi^0 \end{pmatrix} && \text{the Higgs doublet field,} \\ v &= \text{vacuum-expectation-value (vev) of the Higgs field,} \\ L &= \begin{pmatrix} \nu_{\mu L} \\ \mu_L^- \end{pmatrix} && \text{the left-handed lepton doublet of the } 2^{nd} \text{ generation.} \end{aligned}$$

The Wilson coefficient c_6 is suppressed by a high energy scale Λ , which can be interpreted as the energy cutoff for the validity of the EFT.

The operator has been written with the constant term $v^2/2$ subtracted in order to maintain the tree-level relation between the muon mass and the Yukawa coupling

$$m_\mu = \frac{v y_\mu^{\text{SM}}}{\sqrt{2}} \quad (3.6)$$

also in the EFT extension.

3.2.1 Feynman rules

In order to get the Feynman rules from the Lagrangian, we need to choose a parametrization for the four degrees of freedom of the Higgs doublet. When expanding the Higgs doublet around the vev in the Lagrangian, we will get different Feynman rules according to the gauge choice. In any case, the final result for the cross section must be gauge invariant, hence independent of the choice, however one of them may provide significant simplifications depending on the situation.

Unitary gauge

After EW symmetry-breaking, when expanding the new operator of eq. (3.5) in the unitary gauge, i.e. as in (1.16), we get three new vertices involving the muon and Higgs fields:

$$\begin{aligned}
 \mathcal{L}^{(6)} &= \frac{c_6}{\Lambda^2} \left(\phi^\dagger \phi - \frac{v^2}{2} \right) (\bar{L} \phi \mu_R + \text{h.c.}) \\
 &= \frac{c_6}{\Lambda^2} \frac{1}{2} (2vh + h^2) \left(\bar{\mu}_L \frac{v+h}{\sqrt{2}} \mu_R + \text{h.c.} \right) \\
 &= \frac{1}{\sqrt{2}} \frac{c_6}{\Lambda^2} \left(v^2 h + \frac{3}{2} v h^2 + \frac{1}{2} h^3 \right) (\bar{\mu}_L \mu_R + \bar{\mu}_R \mu_L).
 \end{aligned} \tag{3.7}$$

The corresponding Feynman rules are:

$$V_1 = \begin{array}{c} \mu^- \\ \swarrow \\ \bullet \\ \nearrow \\ \mu^+ \end{array} \begin{array}{c} \text{---} h \end{array} = i \frac{c_6}{\Lambda^2} \frac{v^2}{\sqrt{2}}, \tag{3.8}$$

$$V_2 = \begin{array}{c} \mu^- \\ \swarrow \\ \bullet \\ \nearrow \\ \mu^+ \end{array} \begin{array}{c} \text{---} h \\ \text{---} h \end{array} = i \frac{c_6}{\Lambda^2} \frac{3v}{\sqrt{2}}, \tag{3.9}$$

$$V_3 = \begin{array}{c} \mu^- \\ \swarrow \\ \bullet \\ \nearrow \\ \mu^+ \end{array} \begin{array}{c} \text{---} h \\ \text{---} h \\ \text{---} h \end{array} = i \frac{c_6}{\Lambda^2} \frac{3}{\sqrt{2}}. \tag{3.10}$$

The contribution of the first diagram in eq. (3.8) is a Yukawa-like term with a strength given by

$$y_\mu^{\text{NP}} = \frac{c_6 v^2}{\Lambda^2}. \quad (3.11)$$

The new V_2 and V_3 vertices generate a local interaction between muons and 2 or 3 Higgs bosons. All vertices are proportional to the c_6/Λ^2 coupling.

R_ξ gauges

Instead of getting rid of the Goldstone bosons, we can keep them and expand the Lagrangian using the parametrization in (1.15). Hence we now get interactions between μ^- , μ^+ and the three Goldstone bosons, as well as the Higgs:

$$\begin{aligned} \mathcal{L} \supset \frac{c_6}{2\sqrt{2}\Lambda^2} & [(h^2 + 2vh) (\bar{\mu}_L \mu_R + \bar{\mu}_R \mu_L) (v + h) + \\ & (h^2 + 2vh) iG_z (\bar{\mu}_L \mu_R - \bar{\mu}_R \mu_L) + \\ & (2G^+ G^- + G_z^2) (\bar{\mu}_L \mu_R + \bar{\mu}_R \mu_L) (v + h) + \\ & (2G^+ G^- + G_z^2) iG_z (\bar{\mu}_L \mu_R - \bar{\mu}_R \mu_L)]. \end{aligned} \quad (3.12)$$

The + or - sign between $\bar{\mu}_L \mu_R$ and the hermitian conjugate depends on the number of Goldstone bosons. The vertices involving the Higgs only are the same as for the unitary gauge, while for the Goldstone bosons they are:

1 Goldstone

$$\begin{aligned} \mu^- \text{ and } \mu^+ \text{ meeting at a vertex with } G_z \text{ and } h \text{ outgoing} &= \pm \frac{c_6 v}{\Lambda^2 \sqrt{2}} \\ \mu^- \text{ and } \mu^+ \text{ meeting at a vertex with } G^+, G^-, \text{ and } h \text{ outgoing} &= \pm \frac{c_6}{\Lambda^2} \frac{1}{\sqrt{2}} \end{aligned} \quad (3.13)$$

2 Goldstone

$$\begin{aligned} \mu^- \text{ and } \mu^+ \text{ meeting at a vertex with } G^+ \text{ and } G^- \text{ outgoing} &= i \frac{c_6 v}{\Lambda^2 \sqrt{2}} \\ \mu^- \text{ and } \mu^+ \text{ meeting at a vertex with } G^+, G^-, \text{ and } h \text{ outgoing} &= i \frac{c_6}{\Lambda^2} \frac{1}{\sqrt{2}} \\ \mu^- \text{ and } \mu^+ \text{ meeting at a vertex with } G_z \text{ and } G_z \text{ outgoing} &= i \frac{c_6 v}{\Lambda^2 \sqrt{2}} \\ \mu^- \text{ and } \mu^+ \text{ meeting at a vertex with } G_z, G_z, \text{ and } h \text{ outgoing} &= i \frac{c_6}{\Lambda^2} \frac{1}{\sqrt{2}} \end{aligned} \quad (3.14)$$

3 Goldstone

$$\begin{array}{c} \mu^- \\ \nearrow \\ \bullet \\ \nwarrow \\ \mu^+ \end{array} \begin{array}{c} \text{---} G_z \\ \text{---} G^+ \\ \text{---} G^- \end{array} = \pm \frac{c_6}{\Lambda^2} \frac{1}{\sqrt{2}} \qquad \begin{array}{c} \mu^- \\ \nearrow \\ \bullet \\ \nwarrow \\ \mu^+ \end{array} \begin{array}{c} \text{---} G_z \\ \text{---} G_z \\ \text{---} G_z \end{array} = \pm \frac{c_6}{\Lambda^2} \frac{3}{\sqrt{2}} \quad (3.15)$$

As we will see in section 4.2, a non-unitary gauge choice is very useful when we want to study multiboson production in the high-energy limit, since the vertices of eqs. (3.13), (3.14), (3.15) can be used to write the dominant diagrams for certain processes.

3.2.2 EFT vs κ framework

We summarise the main features of the two frameworks, focusing on our theory with the operator in eq. (3.5):

- EFT framework

There are new Feynman rules coming from eqs. (3.7) and (3.12), depending on the gauge choice. All new vertices are proportional to the new physics coupling c_6/Λ^2 .

- κ framework

The new physics effects are not encoded in a specific model, as for the EFT, but they are instead parametrized in a generic coefficient κ_μ modifying the strength of the SM vertex. For the Yukawa coupling this is given by

$$\kappa_\mu \equiv \frac{y_\mu}{y_\mu^{\text{SM}}}. \quad (3.16)$$

There is not any new Feynman rule, the only modification is the strength of the Yukawa vertex.

It is possible to identify a one way mapping between the free parameters of the theories, which in this case are c_6/Λ^2 and κ_μ . In the EFT, the modification of the first diagram to the SM coupling y_μ^{SM} can be written as

$$y_\mu \equiv y_\mu^{\text{SM}} + y_\mu^{\text{NP}} = \frac{\sqrt{2} m_\mu}{v} + \frac{c_6 v^2}{\Lambda^2} \equiv y_\mu^{\text{SM}} \kappa_\mu, \quad (3.17)$$

so that κ_μ is defined as

$$\kappa_\mu \equiv 1 + \frac{c_6}{\Lambda^2} \frac{v^3}{\sqrt{2} m_\mu}. \quad (3.18)$$

For $\kappa_\mu = 1$ we get the Yukawa of the SM. The deviation is proportional to the new coupling c_6/Λ^2 .

Vertices cancellations in the κ framework

The κ framework can be embedded consistently in the SMEFT, when we consider specific processes. It is indeed equivalent to introducing higher dimensional operators and tune their coefficients properly to exactly cancel all the new vertices, except for the Yukawa-like term, which does not receive any higher-order correction. Having subtracted $v^2/2$ from the doublet product, each higher-order operator will start affecting vertices with always a higher number of Higgs bosons.

Introducing the operator in (3.5) we derive the 3 new Feynman rules of eqs. (3.8), (3.9), (3.10) of the SMEFT framework. If we want to introduce only the Yukawa-like vertex V_1 of (3.8), we have to “turn off” the others setting them to 0. This can be done by introducing in the SMEFT higher-dimension operators of the type

$$\mathcal{L}^{(4+2n)} = \frac{c_{4+2n}}{\Lambda^{2n}} \left(\phi^\dagger \phi - \frac{v^2}{2} \right)^n (\bar{L}\phi\mu_R + \text{h.c.}). \quad (3.19)$$

From their expansion, we will find new Feynman rules involving up to $1 + 2n$ Higgs or Goldstone bosons, which we can calibrate in order to cancel properly the extra vertices. We show as an example how the dimension 8 and dimension 10 operators can cancel the vertices in (3.9) and (3.10). Since we want to fix 2 vertices, we need to introduce 2 extra degrees of freedom, c_8 and c_{10}

$$\mathcal{L}^{(8)} = \frac{c_8}{\Lambda^4} \left(\phi^\dagger \phi - \frac{v^2}{2} \right)^2 (\bar{L}\phi\mu_R + \text{h.c.}), \quad (3.20)$$

$$\mathcal{L}^{(10)} = \frac{c_{10}}{\Lambda^6} \left(\phi^\dagger \phi - \frac{v^2}{2} \right)^3 (\bar{L}\phi\mu_R + \text{h.c.}). \quad (3.21)$$

Expanding the Higgs doublet in the unitary gauge as in (1.16), we find

$$\mathcal{L}^{(8)} = \frac{c_8}{\Lambda^4 \sqrt{2}} \frac{1}{4} [4v^3 h^2 + 8v^2 h^3 + 5vh^4 + h^5] (\bar{\mu}_L \mu_R + \bar{\mu}_R \mu_L), \quad (3.22)$$

$$\mathcal{L}^{(10)} = \frac{c_{10}}{\Lambda^6 \sqrt{2}} \frac{1}{8} [8v^4 h^3 + 20v^3 h^4 + 18v^2 h^5 + 7vh^6 + h^7] (\bar{\mu}_L \mu_R + \bar{\mu}_R \mu_L). \quad (3.23)$$

The new Feynman rules for the vertices with 2 and 3 Higgs in (3.9) and (3.10) become

$$V_2 = i 2 \left(\frac{c_6}{\Lambda^2 \sqrt{2}} \frac{3}{2} v + \frac{c_8}{\Lambda^4 \sqrt{2}} v^3 \right), \quad (3.24)$$

$$V_3 = i 6 \left(\frac{c_6}{\Lambda^2 \sqrt{2}} \frac{1}{2} + \frac{c_8}{\Lambda^4 \sqrt{2}} 2v^2 + \frac{c_{10}}{\Lambda^6 \sqrt{2}} v^4 \right). \quad (3.25)$$

Now, imposing $V_2 = 0$ and $V_3 = 0$, we find the required values for c_8 and c_{10} , namely

$$\frac{c_8}{\Lambda^4 \sqrt{2}} = -\frac{3}{2v^2} \frac{c_6}{\Lambda^2 \sqrt{2}}, \quad \frac{c_{10}}{\Lambda^6 \sqrt{2}} = \frac{5}{2v^4} \frac{c_6}{\Lambda^2 \sqrt{2}}. \quad (3.26)$$

It is worth remarking an important consequence of this interpretation. As we can see from the expansions in (3.22) and (3.23), the higher dimensional operators generate vertices with up to 5 and 7 Higgs/Goldstone bosons respectively, which are not present in the 6 dimensional SMEFT. The equivalence between the two frameworks depends on what processes we want to study. For example, in the next chapter we will study the effect of operator on the production of 2, 3, and 4 bosons. In the κ framework, while the vertices $\mu^+ \mu^- n h$, $n \geq 2$ are 0, this is not the case for the contact terms with the Goldstone bosons. The choice of parameters in (3.26) introduces new vertices with 4 Goldstone boson as well that are proportional to c_6 . These vertices generate the dominant amplitudes in the high-energy limit, causing an enhancement with respect to the EFT case in 4 boson production. This result is shown later in section 4.3.2.

Chapter 4

Multiboson production

In section 2.2 we discussed how measuring with high precision the muon Yukawa coupling might give hints on heavy new physics, and that the muon collider could likely be the most suited facility for spotting these deviations. The ultimate goal is now finding processes that are sensitive to BSM effects. Thanks to the high-energy reach of muon colliders, the muon coupling can be directly measured in multiboson production via muon annihilation, leveraging on the energy growth induced by the violation of unitarity [36]. Indeed, as discussed in section 1.2.2, the Higgs field plays a fundamental role in the unitarization of the SM, ensuring that energy-growing contributions are exactly cancelled among the SM amplitudes.

As an example, we can consider the process $\mu^+\mu^- \rightarrow ZZZ$: the amplitudes are shown in Fig. 4.1. In the third diagram, the Higgs couple directly to the muon, hence the amplitude is proportional to the muon mass. The mass dependence of the energy-growing terms arising from the other amplitudes is instead of kinematic origin. The “miraculous” cancellation between dangerous terms is a consequence of the mass generation mechanism of the SM.

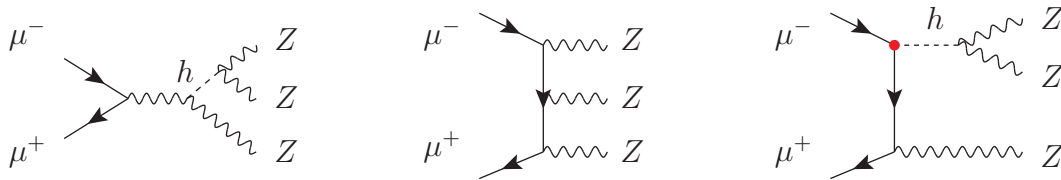


Figure 4.1: The three diagrams contributing to the $\mu^+\mu^- \rightarrow ZZZ$ process. The third diagrams involving the Higgs makes the process sensitive to the muon Yukawa coupling.

If BSM effects are present, they become manifest by disrupting these cancellations, thus

inducing an energy growth in the multiboson production cross section [37]. The deviation from the SM prediction, which is instead unitarity safe, may become important in the multi-TeV range.

The processes considered in this work are the $\mu^+\mu^-$ annihilation into two bosons:

$$hh, hZ, ZZ, W^+W^-, \quad (4.1)$$

three bosons:

$$hhh, hhZ, hZZ, ZZZ, W^+W^-h, W^+W^-Z, \quad (4.2)$$

and four bosons:

$$\begin{aligned} & hhhh, hhhZ, hhZZ, hZZZ, ZZZZ, \\ & W^+W^-hh, W^+W^-hZ, W^+W^-ZZ, W^+W^-W^+W^-, \end{aligned} \quad (4.3)$$

in a range of center-of-mass energy $1 < \sqrt{s} < 30$ TeV.

In absence of a specific new physics model, we parametrize the BSM effects in the EFT framework. The κ framework is also considered for comparison.

All numerical analyses are carried out with MADGRAPH5_AMC@NLO, implementing the EFT and κ frameworks with Feynrules.

4.1 Perturbative expansion in the effective coupling

In both the EFT and κ frameworks, we perturbatively expand the squared amplitude in the new physics coupling c_6/Λ^2 :

$$\begin{aligned} |\mathcal{M}|^2 &= |\mathcal{M}_{\text{SM}}|^2 + 2 \frac{c_6}{\Lambda^2} \text{Re}(\mathcal{M}_{\text{SM}}^* \mathcal{M}_{\text{NP}=1}) + \\ &+ \frac{c_6^2}{\Lambda^4} \left[|\mathcal{M}_{\text{NP}=1}|^2 + 2 \text{Re}(\mathcal{M}_{\text{SM}}^* \mathcal{M}_{\text{NP}=2}) \right] + \\ &+ \dots \end{aligned} \quad (4.4)$$

where $\mathcal{M}_{\text{NP}=i}$ is the matrix element with i insertions of c_6 , thus $\mathcal{M}_{\text{NP}=i} \sim (c_6/\Lambda^2)^i$. In the expansion in (4.4) this dependence is extracted from the matrix element.

It is worth noticing that the first order contribution - linear in c_6 - is unambiguous, in the sense that there is only one type of contribution given by the interference between SM amplitudes and those with only one new physics insertion. Going to higher orders instead, we get different results cutting the expansion in \mathcal{M} rather than in $|\mathcal{M}|^2$.

In what follows we denote the linear expansion (hence containing up to 1 c_6) as NP1, the quadratic expansion, involving only up to $\mathcal{M}_{\text{NP}=1}$, as NP2, and the expansion in which we keep all new physics terms as NPall.

4.1.1 First order suppression

Since the new physics contribution appears as a perturbative expansion, as shown in eq. (4.4), we expect that each term brings a lower order correction to the previous ones, being more suppressed by an extra factor c_6/Λ^2 . Actually, if the coefficients of the expansion differ of several orders of magnitude, the hierarchy of the terms might be altered. This is indeed what happens to the first order contribution: although we expect it to be more relevant than the second, it is actually suppressed due to a hierarchy in the polarized amplitudes. Hence, even though truncating the expansion at first order may seem the most sensible choice because of its unambiguity, it would cut away the dominant corrections.

In order to better understand the NP1 suppression, we can consider again the example of ZZ production discussed in section 1.2.2 and analyse the polarized cross sections, focusing on the production of longitudinally polarized bosons Z_L . This is a particularly simple case since, as shown later, the EFT and κ framework coincide. Moreover, we work in the unitary gauge, since the new physics contributes in a single diagram.

Unitarity cancellations in the SM

In the SM, there are three types of diagrams contributing, as shown in Fig. 4.2.

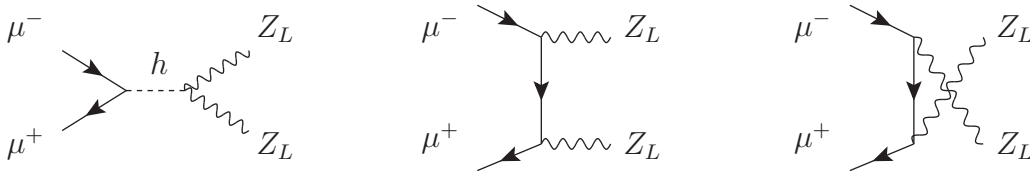


Figure 4.2: The three SM diagrams contributing to $\mu^-\mu^+ \rightarrow Z_L Z_L$.

As already discussed in section 1.2.2, longitudinal polarizations are the ones responsible for the potential unitarity violation at high energies, but cancellations between the SM polarized amplitudes (presented in Table 4.1) ensure that the energy growth is controlled.

$\lambda^- \lambda^+$	\mathcal{M}_s	\mathcal{M}_{t+u}
RL, LR	0	a constant $A(\lambda^+, \lambda^-)$
RR, LL	(a constant B) $\pm \sqrt{2}G_F m_\mu \sqrt{s}$	(a constant C) $\mp \sqrt{2}G_F m_\mu \sqrt{s}$

Table 4.1: High-energy limit of the matrix element for the production of longitudinally polarized Z . λ^- and λ^+ are the helicities of μ^- and μ^+ respectively. The energy-dependent terms are computed using Goldstone Bosons Equivalence theorem.

We observe that the scattering between opposite helicities is not problematic, while cancellations happen between amplitudes for same helicity configurations. Moreover, the s channel does not contribute to $\sigma(LR)$ and $\sigma(RL)$.

In Table 4.2 are displayed the polarized cross sections in pb at $\sqrt{s} = 30$ TeV from MadGraph, for longitudinally polarized Z and for all polarizations of Z . For the Z_L cross section, the contributions from different diagrams are evaluated separately, in order to highlight the diverging contributions that are cancelled.

In the production of longitudinally polarized bosons, as expected, for $\sigma(LR)$ and $\sigma(RL)$ the s channel gives 0 contribution. However, looking at $\sigma(RR)$ and $\sigma(LL)$, we see how the Higgs plays a fundamental role in the cancellation of divergences. Indeed, without the Higgs - and the s channel diagram - the cross section is 10 orders larger than observed in the SM with all three diagrams. What happens instead is that the diverging contributions of the s channel and the $u + t$ channels disappear when summing the matrix elements, thus leaving a very small, constant contribution.

Focusing on the overall contributions from all channels, in the SM we observe a natural suppression of 2 orders of magnitude between scattering among same and opposite polarizations. Moreover, longitudinal polarizations are themselves suppressed with respect to transverse polarizations of several orders of magnitude actually, as observed by comparing first and fourth columns.

This is the key to understand the suppression of the linear expansion NP1 in the EFT (and κ) framework.

Energy growth in EFT and κ frameworks

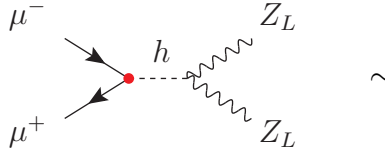
We consider the situation in which the correction to the Yukawa coupling is exactly equal to $-y_\mu^{\text{SM}}$, such that the Yukawa vertex is cancelled by setting $\kappa_\mu = 0$. Imposing this condition we get

$$\frac{c_6}{\Lambda^2} = \frac{\sqrt{2} m_\mu}{v^3} \simeq 1.00107 \cdot 10^{-8} \text{ GeV} \quad (4.5)$$

$\lambda^- \lambda^+$	$\sigma(\rightarrow Z_L Z_L)$			$\sigma(\rightarrow ZZ)$ (pb)
	$ s + t + u ^2$	$ t + u ^2$	$ s ^2$	$ s + t + u ^2$
LR	$5.265 \cdot 10^{-13}$	$5.265 \cdot 10^{-13}$	0	$1.092 \cdot 10^{-3}$
RL	$2.431 \cdot 10^{-13}$	$2.425 \cdot 10^{-13}$	0	$0.6516 \cdot 10^{-3}$
RR	$2.362 \cdot 10^{-15}$	$1.179 \cdot 10^{-5}$	$1.173 \cdot 10^{-5}$	$4.936 \cdot 10^{-6}$
LL	$2.366 \cdot 10^{-15}$	$1.175 \cdot 10^{-5}$	$1.175 \cdot 10^{-5}$	$5.043 \cdot 10^{-6}$

Table 4.2: Contributions of the initial polarizations to σ in the SM, for the production of both polarized and unpolarized vectors. The first three columns report the values from MadGraph at $\sqrt{s} = 30$ TeV, in pb, considering all three channels, only t and u , and only s . The fourth column shows the values for all the Z polarizations.

which, setting for example the new physics scale at $\Lambda = 1$ TeV, selects $c_6 = 0.01$. In addition to the previous diagrams of Fig. 4.2, there is now one extra diagram contributing:



$$B' \mp \frac{c_6}{\Lambda^2} \frac{v}{\sqrt{2}} \sqrt{s} \quad \begin{array}{l} \lambda^- \lambda^+ = RL, LR \\ \lambda^- \lambda^+ = RR, LL \end{array} \quad (4.6)$$

where B' is a constant, obtained using GBE theorem. Since there is not any new diagram containing the vertices V_2 and V_3 of eqs. (3.9) and (3.10), the EFT and κ frameworks coincide for this process. For $\kappa_\mu = 0$, $B' = -B$ since the new physics vertex V_1 is $\sim c_6 v^2 / \Lambda^2 = -y_\mu^{\text{SM}}$.

Notice that this new matrix element is $\neq 0$ only for opposite helicities, thus $\sigma_{\text{NP}}(LR)$ and $\sigma_{\text{NP}}(RL)$ are exactly the same as in the SM.

This is true at every perturbative order in the new physics coefficient expansion and in particular it is true for NP1 and NP2. Therefore these initial polarizations are not responsible for the growth in energy, which is instead due to the new diagram (only present for opposite helicities) containing a term that grows with \sqrt{s} and does not cancel. For NP1 we are introducing the interference among the new diagram and the ones of the SM

$$|\mathcal{M}_{\text{NP1}}(RR, LL)|^2 = |\mathcal{M}_{\text{SM}}(RR, LL)|^2 + 2 \left[B' \mp \frac{c_6}{\Lambda^2} \frac{v}{\sqrt{2}} \sqrt{s} \right] \cdot [B + C], \quad (4.7)$$

while in NP2 we add on top of this the square of the new diagram, thus introducing a growth with s instead of \sqrt{s} :

$$|\mathcal{M}_{\text{NP2}}(RR, LL)|^2 = |\mathcal{M}_{\text{NP1}}(RR, LL)|^2 + \left[B' \mp \frac{c_6}{\Lambda^2} \frac{v}{\sqrt{2}} \sqrt{s} \right]^2. \quad (4.8)$$

The values for $\sigma(RR) = \sigma(LL)$ for the production of $Z_L Z_L$, in pb, are reported in Table 4.3. The fact that σ_{NP2} is equivalent to the σ_{SM} without s channel is a consequence of choosing $\kappa_\mu = 0$. Indeed

$$|\mathcal{M}_{\text{SM}}^{t+u}|^2 = \left(C \mp \sqrt{2} G_F m_\mu \sqrt{s} \right)^2 \quad (4.9)$$

	SM	NP1	NP2
$\sigma(RR), \sigma(LL)$	$2.36 \cdot 10^{-15}$	$2.62 \cdot 10^{-11}$	$1.18 \cdot 10^{-5}$

Table 4.3: $\sigma(\rightarrow Z_L Z_L)$ (pb) from MadGraph for polarized muons with same helicities at $\sqrt{s} = 30$ TeV, in the SM and EFT/ κ frameworks at first and second order in the new physics coupling.

while imposing $B' = -B$

$$\begin{aligned}
|\mathcal{M}_{\text{NP2}}|^2 &= (B + C)^2 + 2 \left(-B \mp \sqrt{2} G_F m_\mu \sqrt{s} \right) (B + C) + \left(-B \mp \sqrt{2} G_F m_\mu \sqrt{s} \right)^2 \\
&= (B^2 + C^2 + 2BC) + 2 \left(-B^2 - BC \mp B \sqrt{2} G_F m_\mu \sqrt{s} \mp C \sqrt{2} G_F m_\mu \sqrt{s} \right) \\
&\quad + \left(B^2 + 2 G_F^2 m_\mu^2 s \pm 2 B \sqrt{2} G_F m_\mu \sqrt{s} \right) \\
&= C^2 \mp 2 C \sqrt{2} G_F m_\mu \sqrt{s} + 2 G_F^2 m_\mu^2 s \\
&= \left(C \mp \sqrt{2} G_F m_\mu \sqrt{s} \right)^2.
\end{aligned} \tag{4.10}$$

Looking at NP1 in Table 4.3, we notice that the contribute of $\sigma_{\text{NP1}}(RR)$ and $\sigma_{\text{NP1}}(LL)$ to the production of longitudinally polarized bosons is dominant with respect to the other initial polarizations $\sigma_{\text{NP1}}(RL)$ and $\sigma_{\text{NP1}}(LR)$, which are of order 10^{-13} as in the SM. So the growth in energy would actually be visible if we observed longitudinal polarizations only. However, as shown in Table 4.2, longitudinal polarizations are very suppressed with respect to the transversal ones, thus becoming dominant only at high energies in the EFT/ κ framework. For this reason the growth in NP1 is not visible, but for NP2 it gives relevant contributions that can be observed.

Unpolarized cross section

$\lambda^- \lambda^+$	SM	NP1	NP2
LR	$1.092 \cdot 10^{-3}$	$1.092 \cdot 10^{-3}$	$1.092 \cdot 10^{-3}$
RL	$6.516 \cdot 10^{-4}$	$6.516 \cdot 10^{-4}$	$6.506 \cdot 10^{-4}$
RR	$4.936 \cdot 10^{-6}$	$4.935 \cdot 10^{-6}$	$1.162 \cdot 10^{-5}$
LL	$5.043 \cdot 10^{-6}$	$5.074 \cdot 10^{-6}$	$1.192 \cdot 10^{-5}$
unpolarized	$4.384 \cdot 10^{-4}$	$4.385 \cdot 10^{-4}$	$4.416 \cdot 10^{-4}$

Table 4.4: $\sigma(\rightarrow ZZ)$ (pb) from MadGraph for polarized muons at $\sqrt{s} = 30$ TeV, in the SM and EFT/ κ frameworks at first and second order in the new physics coupling. The last line shows the unpolarized cross section in each framework, i.e. averaged over initial polarizations.

In Table 4.4 are reported the cross sections in pb, for the production of unpolarized Z bosons, considering polarized and unpolarized muons. For NP2, the longitudinal

polarizations contribute to order 10^{-5} , so they are significant at 30 TeV, even though for this process they are not dominant yet over transversal polarizations.

4.1.2 Second order is dominant

Since the second order terms are greater than the first ones, we must be careful on which order to cut the expansion. Is NP2 dominant over the higher order terms, or we should consider even more contributions? It turns out that if we keep all terms in the expansion, as in NPall, the cross sections are equivalent to NP2. Recall that in NP2 we keep in the squared amplitude only contributions up to order 2 overall, with maximum one new physics contribution per diagram. This means that the high energy limit is uniquely dominated by certain diagrams containing only one anomalous vertex. This is clear for 2 and 3 boson production, since in these processes the Feynman gauge allows to write diagrams containing only the contact vertices V_2 and V_3 of eqs. (3.9) and (3.10) without any propagator. However, this is no longer the case for 4 boson production, given that all diagrams now contain one or more internal propagators. The asymptotic limit is therefore non-trivial.

In the Feynman gauge the diagrams relevant for this discussion are similar for vector and Higgs bosons, because the Higgs and Goldstone bosons couple to the muons in similar way, so we can just analyse the 4 Higgs production.

EFT framework

We expect the dominant diagrams to be those containing the minimal number of internal propagators, which is one: the candidate diagrams to dominate are shown in Fig. 4.3. We can define two types of these potentially dominating diagrams: those with the fermion propagator and those with the Higgs propagator. The former can have also 2 new vertices, as for (a) and (b): they are present for NPall but not for NP2. The latter, with the Higgs propagator, have only one new physics insertion, hence their contribution is the same in NP2 and NPall.

The fact that NP2 and PNall are equivalent suggests that the diagrams with the Higgs propagator only are dominant, and this is indeed the case. In Tab. 4.5 are presented the values for the cross section of $\mu^+\mu^- \rightarrow hhhh$ at $\sqrt{s} = 30$ TeV in the EFT framework, with $\Lambda = 2$ TeV and $c_6 = 0.01$, corresponding approximately to a value of $\kappa_\mu = 3/4$. The diagrams with the muon propagator are extremely suppressed compared to the others. Indeed, instead of a Higgs self coupling they contain one Higgs-muon coupling, which is suppressed by the c_6/Λ^2 dependence. On the other hand, the Higgs self coupling λ is $\sim 1/8$, around two orders of magnitude larger than the anomalous vertices in diagrams (a) and (b): this determines the dominant behavior of diagrams (d) and (e).

κ framework

In this framework the vertices V_2 and V_3 of eqs. (3.9) and (3.10) are turned off, meaning that the diagrams which are dominating in the EFT framework are not present. However

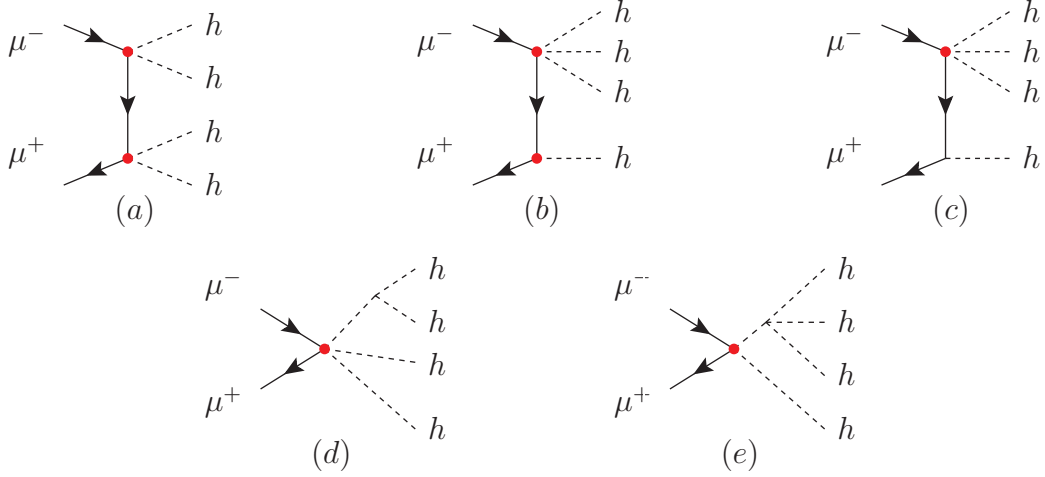


Figure 4.3: Diagrams containing only one propagator for the $\mu^+\mu^- \rightarrow hhhh$ process, in the EFT framework. Amplitudes (a) and (b) are present in NPall, but not in NP2. The high-energy behavior is however determined by amplitudes (d) and (e).

	NP2	NPall
total σ	$2.6932 \cdot 10^{-7}$	$2.6932 \cdot 10^{-7}$
diagrams without μ propagator	$6.689 \cdot 10^{-7}$	$6.689 \cdot 10^{-7}$
diagrams without h propagator	$1.531 \cdot 10^{-13}$	$6.597 \cdot 10^{-14}$

Table 4.5: σ (pb) at $\sqrt{s} = 30$ TeV in the EFT framework, with $\Lambda = 2$ TeV and $c_6 = 0.01$ at second and all orders in the new physics coupling. Diagrams without Higgs propagator are dominated by (a), (b) and (c) of Fig. 4.3, while (d) and (e) are the dominant contributions to diagrams without muon propagator.

the situation is still similar. In this case the diagrams contain at least two internal propagators and again we can define two types of them, shown in Fig. 4.4: those with two Higgs propagators, (a) and (b), and those with one Higgs and one fermion propagator, (c), (d), (e) and (f). Diagram (f) is present for NPall but not for NP2. However diagrams (a) and (b) are dominant over the others, since they have a Higgs self coupling instead of a Higgs-muon coupling.

Tab. 4.6 shows how diagrams without the muon propagator, like (a) and (b), represent the most relevant contribution to the total cross section, explaining why also in this framework we can truncate the new physics expansion at second order in c_6/Λ^2 .

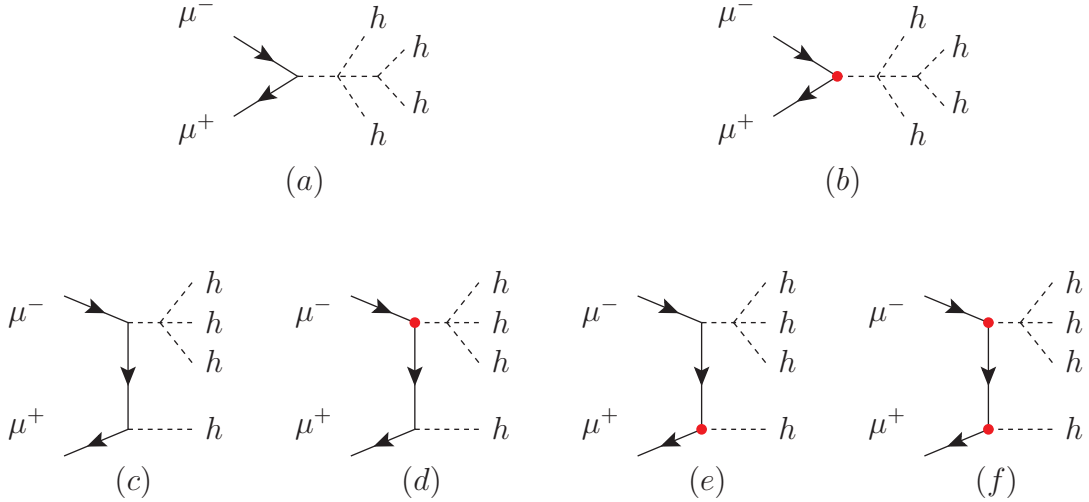


Figure 4.4: Diagrams containing only two propagators for the $\mu^+\mu^- \rightarrow hhhh$ process, in the κ framework. Amplitude (f) is present in NPall, but not in NP2. The high-energy behavior is however determined by amplitudes (a) and (b).

	NP2	NPall
total σ	$7.305 \cdot 10^{-16}$	$7.302 \cdot 10^{-16}$
diagrams without μ propagator	$7.268 \cdot 10^{-16}$	$7.268 \cdot 10^{-16}$

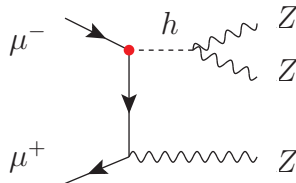
Table 4.6: σ (pb) at $\sqrt{s} = 30$ TeV in the κ framework, with $\Lambda = 2$ TeV and $c_6 = 0.01$ at second and all orders in the new physics coupling. Diagrams without muon propagator are dominated by (a) and (b) of Fig. 4.4. The extreme suppression of the κ framework with respect to the EFT is due to the fact that the diagrams of Fig. 4.4 are also present in the EFT, but they are subdominant with respect to the ones of Fig. 4.3.

4.2 High-energy behavior for multiboson production

In the SMEFT framework, two and three boson production processes are dominated in the high-energy limit by a single diagram. Indeed, using GBE Theorem, the longitudinal polarizations are approximated at high scales by the Goldstone bosons. Therefore we have that certain diagrams do not present internal propagators [38], so we can easily derive their energy dependence and compare the theoretical predictions with the numerical simulations. The two contact vertices (3.9) and (3.10) are responsible for the dominant diagrams for the 2 and 3 Higgs production respectively at high energies. Contrary to other channels, they contribute to diagrams that do not contain any propagator and consequently are not suppressed. In the other processes instead, the high-energy behavior

is not as trivial, but it is instead determined by the combined contributions of many diagrams.

Take as an example the $\mu^+\mu^- \rightarrow ZZZ$ process. The high-energy behavior is the result of the combination of the diagrams in Fig. 4.1, which are the SM ones, plus a new diagram involving the V_1 vertex:



In this case it is not clear a priori which diagrams are dominant, and the only way to determine the cross section is to carry out the calculation with all the diagrams.

In this section we analyse the energy growth induced by the violation of unitarity in SMEFT, as it plays a crucial role in the sensitivity of multiboson production.

4.2.1 Analytical predictions

The differential cross section is given by

$$d\sigma = \frac{|\mathcal{M}|_{\text{unpol}}^2}{\Phi} d\Pi_{\text{LIPS}}. \quad (4.11)$$

In this expression

$$\Phi = (2E_A)(2E_B)|\vec{v}_A - \vec{v}_B| \quad (4.12)$$

is the flux of the 2 colliding beams A and B with velocities \vec{v}_A and \vec{v}_B , $|\mathcal{M}|_{\text{unpol}}^2$ is the unpolarized matrix element, while $d\Pi_{\text{LIPS}}$ is the Lorentz invariant phase space volume element

$$d\Pi_{\text{LIPS}} = \prod_f \frac{d^3k_f}{(2\pi)^3 2E_f} (2\pi)^4 \delta^{(4)}\left(\sum_f k_f - p\right) \quad (4.13)$$

where $k_f = (E_f, \vec{k}_f)$ are the final-state momenta and p is the total initial momentum. Considering the center-of-mass frame and massless particles in the initial state (we are interested in the high-energy limit), the flux is just $\Phi = 2s$, where $s = E_{\text{CM}}^2$ is the Mandelstam invariant and $E_A + E_B = E_{\text{CM}}$ is the collision energy in the center-of-mass frame. Denoting as V the Feynman rule of the vertex for the contact term, we can approximate the matrix element for longitudinally polarized vectors in the high-energy limit, averaged over muons polarizations, as

$$|\mathcal{M}|_{\text{unpol}}^2 = \frac{1}{4}|V|^2 2s = \frac{s}{2}|V|^2. \quad (4.14)$$

Notice that the mass dimension of V is -2 for triboson production, while it is -1 in diboson production. Indeed, by expanding the 3 Higgs doublets as in (3.12), we get for each vertex 3 insertions of bosons/vev. This restores the correct dimension of σ , since

$$\sigma = \frac{1}{2s} \frac{s |V|^2}{2} \Pi_{\text{LIPS}}, \quad (4.15)$$

and given that phase space is adimensional for two particles, while it has dimension 2 for three particles.

Cross section for 2 to 2 scattering

The 2-particle phase space is given by

$$\begin{aligned} d\Pi_{\text{LIPS}}^{(2)} &= \frac{d^3k_1 d^3k_2}{(2\pi)^6 (2E_1)(2E_2)} (2\pi)^4 \delta^{(4)}(k_1 + k_2 - p) \\ &= \frac{d^3p_f}{(2\pi)^3} \frac{1}{4 E_1 E_2} (2\pi) \delta(E_1 + E_2 - E_{\text{CM}}) \\ &= d\Omega \frac{p_f^2 dp_f}{16 \pi^2} \frac{1}{E_1 E_2} \delta(E_1 + E_2 - E_{\text{CM}}). \end{aligned} \quad (4.16)$$

where $\vec{p}_f = \vec{k}_1 = -\vec{k}_2$. Changing variable

$$x = E_1 + E_2 - E_{\text{CM}} = \sqrt{p_f^2 + m_1^2} + \sqrt{p_f^2 + m_2^2} - E_{\text{CM}}, \quad (4.17)$$

$$dx = \frac{E_{\text{CM}}}{E_1 E_2} p_f dp_f \quad (4.18)$$

the phase space integral becomes

$$\int d\Pi_{\text{LIPS}}^{(2)} = \int \frac{d\Omega}{16 \pi^2} \int_{m_1+m_2-E_{\text{CM}}}^{\infty} dx \frac{p_f}{E_{\text{CM}}} \delta(x) = \int \frac{d\Omega}{16 \pi^2} \frac{p_f}{E_{\text{CM}}} \theta(E_{\text{CM}} - m_1 - m_2). \quad (4.19)$$

For massless particles in the final state $E_{\text{CM}} = 2p_f$, hence the asymptotic behavior of the cross section is

$$\sigma^{(2)} = \frac{|\mathcal{M}|^2}{2s} \frac{4\pi}{32\pi^2} = \frac{1}{16 \pi s} \frac{s |V|^2}{2} = \frac{|V|^2}{32 \pi} \sim \text{constant}. \quad (4.20)$$

Cross section for 2 to 3 scattering

The 3-body phase space is

$$\begin{aligned} d\Pi_{\text{LIPS}}^{(3)} &= \frac{d^3k_1 d^3k_2 d^3k_3}{(2\pi)^9 (2E_1)(2E_2)(2E_3)} (2\pi)^4 \delta^{(4)}(k_1 + k_2 + k_3 - p) \\ &= \frac{d^3k_1 d^3k_2}{(2\pi)^6 (2E_1)(2E_2)(2E_3)} (2\pi) \delta(E_1 + E_2 + E_3 - E_{\text{CM}}) \end{aligned} \quad (4.21)$$

where we integrated out \vec{k}_3 with $\delta^{(3)}$. The measure in spherical coordinates becomes

$$d^3k_1 d^3k_2 = k_1^2 dk_1 k_2^2 dk_2 d\Omega_1 d\Omega_{12}, \quad (4.22)$$

where $d\Omega_1$ is the spherical integral measure associated with k_1 and it can be integrated over giving 4π , while $d\Omega_{12}$ is the spherical integral measure of the relative angle between \vec{k}_1 and \vec{k}_2 . However, E_3 is not independent of θ_{12} :

$$E_3 = \sqrt{\vec{k}_3^2} \Big|_{\vec{k}_3 = -(\vec{k}_1 + \vec{k}_2)} = \sqrt{\vec{k}_1^2 + \vec{k}_2^2 + 2\vec{k}_1 \cdot \vec{k}_2} = \sqrt{E_1^2 + E_2^2 + 2k_1 k_2 \cos \theta_{12}}. \quad (4.23)$$

We use the properties of the delta function

$$\delta(E_{\text{CM}} - E_1 - E_2 - E_3) = \frac{E_3}{E_1 E_2} \delta\left(\cos \theta_{12} - \frac{E_3^2 - E_1^2 - E_2^2}{2k_1 k_2}\right), \quad (4.24)$$

so that the phase space integral becomes

$$\begin{aligned} \int d\Pi_{\text{LIPS}}^{(3)} &= \int \frac{k_1^2 dk_1 k_2^2 dk_2}{(2\pi)^6 2E_1 2E_2 2E_3} 16\pi^3 \int d\cos \theta_{12} \frac{E_3}{E_1 E_2} \delta\left(\cos \theta_{12} - \frac{E_3^2 - E_1^2 - E_2^2}{2k_1 k_2}\right) \\ &= \frac{1}{32\pi^3} \int dE_1 dE_2. \end{aligned} \quad (4.25)$$

Finally, changing variables

$$x_i = \frac{2E_i}{p}, \quad dx_i = \frac{2}{p} dE_i \quad (4.26)$$

we get

$$\int d\Pi_{\text{LIPS}}^{(3)} = \frac{s}{128\pi^3} \int_0^1 dx_1 \int_{1-x_1}^1 dx_2 = \frac{s}{2 \cdot 128\pi^3}, \quad (4.27)$$

and the total cross section is

$$\sigma^{(3)} = \frac{1}{2s} \frac{s}{2} |V|^2 \frac{s}{2 \cdot 128\pi^3} = |V|^2 \frac{s}{1024\pi^3}. \quad (4.28)$$

Theoretical predictions for longitudinally polarized vectors

Summarising the above results, we can express the high-energy limit of the cross section of Higgs and longitudinally polarized W^+ , W^- , Z , respectively for diboson and triboson production, as

$$\sigma^{(2)} = I_2 |V|^2, \quad I_2 = \frac{1}{32\pi}, \quad (4.29)$$

$$\sigma^{(3)} = I_3(s) |V|^2, \quad I_3(s) = \frac{s}{1024\pi^3}, \quad (4.30)$$

namely an asymptotically constant trend for the former, and a growth with $s \sim E_{\text{CM}}^2$ for the latter.

Substituting the values for V from section 3.2.1, we find for the diboson production

$$\sigma(ZZ) = I_2 \frac{1}{2} v^2 \left(\frac{c_6}{\Lambda^2} \right)^2 \frac{1}{2}, \quad (4.31)$$

$$\sigma(hh) = I_2 \frac{9}{2} v^2 \left(\frac{c_6}{\Lambda^2} \right)^2 \frac{1}{2} = 9 \sigma(ZZ), \quad (4.32)$$

$$\sigma(hZ) = I_2 \frac{1}{2} v^2 \left(\frac{c_6}{\Lambda^2} \right)^2 = 2 \sigma(ZZ), \quad (4.33)$$

$$\sigma(W^+W^-) = I_2 \frac{1}{2} v^2 \left(\frac{c_6}{\Lambda^2} \right)^2 = 2 \sigma(ZZ) \quad (4.34)$$

and for the triboson production

$$\sigma(hZZ) = \sigma(hhZ) = I_3(s) \frac{1}{2} \left(\frac{c_6}{\Lambda^2} \right)^2 \frac{1}{2}, \quad (4.35)$$

$$\sigma(hhh) = \sigma(ZZZ) = I_3(s) \frac{9}{2} \left(\frac{c_6}{\Lambda^2} \right)^2 \frac{1}{6} = 3 \sigma(hZZ), \quad (4.36)$$

$$\sigma(W^+W^-h) = \sigma(W^+W^-Z) = I_3(s) \frac{1}{2} v^2 \left(\frac{c_6}{\Lambda^2} \right)^2 = 2 \sigma(hZZ). \quad (4.37)$$

4.2.2 Numerical results

The predicted asymptotic behaviors can be compared with the exact results from the MadGraph simulation, in the cases of both unpolarized and longitudinally polarized vector bosons. The perturbative expansion in (c_6/Λ^2) of the squared amplitude is truncated at second order, as discussed in section 4.1. The situation we consider is that in which $\kappa_\mu = 0$ equivalent to setting the new physics scale at $\Lambda=1$ TeV and $c_6 = 0.01$, as in eq. 4.5.

Asymptotic behavior for longitudinal polarizations

The plots in Figure 4.6 show the production of two and three bosons, considering only the longitudinal polarizations.

As expected, in general, the high-energy limit is well approximated by the formulas (4.20) and (4.28). However, from the plots, we can make the following observations:

- $\sigma(hZ)$ and $\sigma(W^+W^-)$ should be both approximated asymptotically by (4.33) and (4.34), although this does not appear as clearly as for the other processes. The effect of the new EFT operator to the cross section is indeed to introduce terms

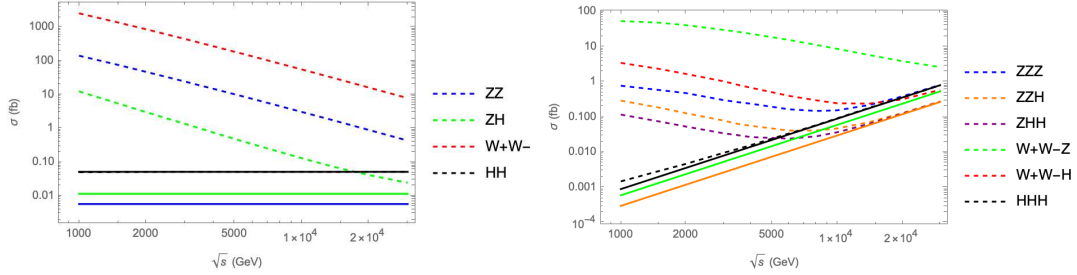


Figure 4.5: Cross section for boson production including all polarizations, as a function of CM energy, in the EFT framework. The dashed lines are for $c_6 = 0.01$ and $\Lambda=1$ TeV, up to second order in (c_6/Λ^2) ; the solid lines are the asymptotic behaviors predicted by (4.20) and (4.28).

proportional to $(c_6/\Lambda^2)^n$, where n is the order of the perturbative expansion, on top of the SM value

$$\sigma = \sigma_{\text{SM}} + \frac{c_6}{\Lambda^2} \sigma_1 + \left(\frac{c_6}{\Lambda^2}\right)^2 \sigma_2 + \mathcal{O}\left(\frac{c_6^3}{\Lambda^6}\right). \quad (4.38)$$

σ_{SM} goes to 0 as $1/s$, while the new physics terms violate unitarity. The difference for these two processes is that their σ_{SM} are much larger than for the other processes, hence the growth induced by unitarity violation becomes dominant at higher energies. In fact the new physics induces

$$\sigma \sim \frac{A}{s} + \text{constant} \quad (4.39)$$

where the constant A is larger for W^+W^- and hZ than for the other processes.

- $\sigma(hh)$ is flat. The reason is that the SM values for double Higgs production cross section are extremely small, therefore in this case the constant contribution is already dominant in this energy range.

Overall asymptotic behavior

So far we have considered only longitudinally polarized vector bosons, in order to verify the equivalence theorem. However, experimentally, the observed final state will include all the polarizations. We can therefore compare the total cross sections for the same processes with the asymptotic behavior, as shown in Fig. 4.5. The energy growth appearing in the EFT is caused by unitarity breaking for longitudinal polarizations, which determine the asymptotic limit. It is still true that, at a certain energy, the asymptotic behavior will start to dominate, however it has to overcome the contributions of all the

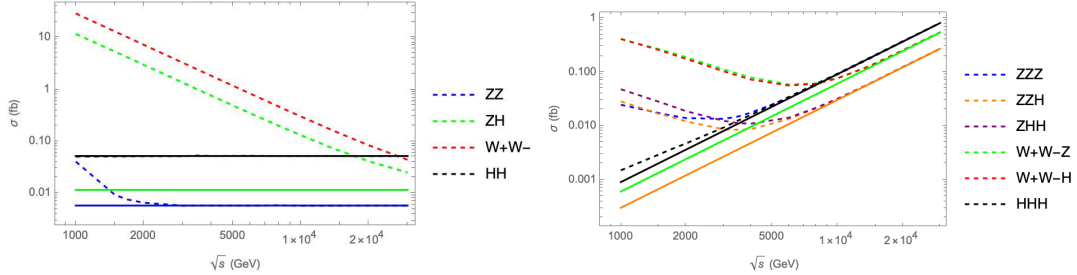


Figure 4.6: Cross section for the production of longitudinally polarized bosons as a function of CM energy, in the EFT. The dashed lines are for $c_6 = 0.01$ and $\Lambda=1$ TeV, up to second order in (c_6/Λ^2) ; the solid lines are the asymptotic behaviors predicted by (4.20) and (4.28).

other polarizations, which are unaffected by the growth. Indeed, the energy at which the longitudinal polarizations become dominant is larger than 30 TeV for diboson production, and is over 10 TeV for triboson production.

For the double and triple Higgs, being scalars, actually nothing changes with respect to the previous case.

4.3 Results

We investigate here in detail multiboson production considering the situation in which the correction to the Yukawa coupling is exactly equal to $-y_\mu^{\text{SM}}$, such that the Yukawa vertex is cancelled. This corresponds to setting $\kappa_\mu = 0$, i.e. $\Lambda = 1$ TeV and $c_6 = 0.01$, as in eq. (4.5).

Since they present very different features, we treat separately the pure multi-Higgs production (i.e. $\mu^- \mu^+ \rightarrow hh, hhh, hhhh$) from the other multiboson channels. In all processes we analyse the EFT and κ frameworks comparing NP1, NP2 and NPall.

4.3.1 EFT framework

Tables 4.7 and 4.8 in the Appendix 4.3.2 show respectively the SM and EFT values for the cross sections.

Vector boson production

The plots comparing the SM results with the NP2-EFT values are reported in Fig. 4.7 for two, three and four boson production respectively. All the processes considered involve at least one vector boson in the final state.

For diboson production, the deviation from the SM cross section is barely visible for Zh , which has indeed the lowest value of σ_{SM} , while it is undetectable for ZZ and W^+W^- . The constant asymptotic behavior induced by longitudinal polarizations is dominated by the SM contribution. On the other hand, the energy growth is more visible for three and four boson production since the relative growth with respect to the SM case is higher, as discussed in section 4.2 and the EFT contributions become dominant at lower energies.

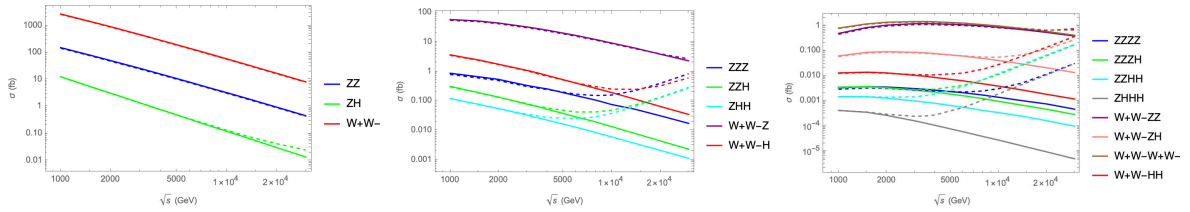


Figure 4.7: Cross section (in fb) for two, three and four boson production in the EFT framework, NP2 (dashed lines) and in the SM (solid lines), as functions of \sqrt{s} (GeV).

Multi-Higgs production

The multi-Higgs production shows a very different behavior and it requires a different discussion from section 4.1.1, since it is no longer true that the interference with the SM amplitude is suppressed. When a vector boson is produced, the scattering of muons with opposite helicities is dominant over that with same helicities (see for instance Table 4.4). For multi-Higgs production, the Higgs only couple to the fermions through Yukawa interaction and it is no longer true that scattering between opposite helicities dominate over the others. Hence the energy enhancement in the unpolarized cross section is significant at all orders in the new physics expansion, and it overcomes the very small values of σ_{SM} already at first order. In fact, for NP1 the absolute value of the new physics correction is larger than the SM value, and being the interference with SM negative, the total σ is itself negative. In NP2 we observe again that the second order terms dominate over the linear one.

In Fig. 4.8 the plots for multi-Higgs production present the comparison between the SM and the EFT frameworks. Being the SM cross section very small, the energy enhancement is already significant at 1 TeV. For example, for the two Higgs production the flat asymptotic behavior is dominant over σ_{SM} and is clearly visible over the entire energy range. This suggests that multi-Higgs production might be the most sensitive process to BSM effects. For comparison, in Fig. 4.8 are reported the most energy enhanced processes containing at least one vector boson: the deviation for the multi-Higgs production is much stronger, resulting in comparable values to the vector boson production. In particular, three and four Higgs production processes present the strongest growth relative to the SM, and three Higgs production has the highest cross section.

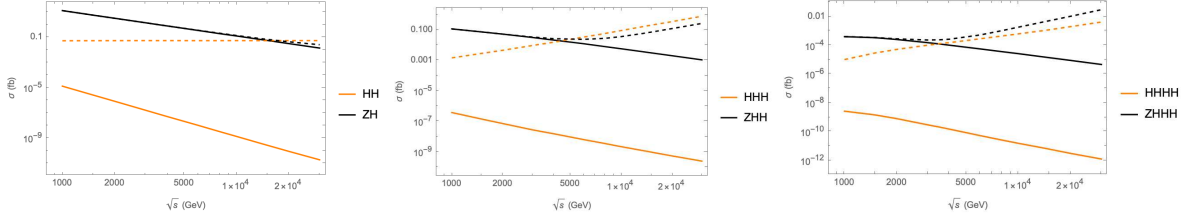


Figure 4.8: Cross sections for the production of two, three and four Higgs boson in the EFT framework at second order in the new physics coupling (dashed lines) and in the SM (solid lines), as functions of \sqrt{s} (GeV). The black plots, for comparison, represent the most sensitive process involving vectorial final state.

4.3.2 κ framework

In Table 4.9 in the Appendix 4.3.2 are reported the values of the cross sections for NP2 in this framework.

Vector boson production

In this framework, the contact vertices V_2 (3.9) and V_3 (3.10) are “turned off”. This procedure breaks unitarity cancellations even more, thus the growth in energy in multiboson production is stronger than for the EFT framework. Indeed, as shown in section 3.2.2, this condition is realised in the EFT by introducing the dimension 8 and 10 operators in (3.20) and (3.21). If we now expand them keeping the Goldstone bosons, as we did for the dimension 6 operator in (3.12), we get new contact vertices for the Goldstone that do not cancel. In particular, we are introducing contact vertices with 4 Goldstone bosons, yielding the dominant diagrams for four boson production, similarly to V_2 and V_3 for two and three bosons. Consequently, the energy enhancement is clearly visible in four boson production.

All the considerations previously made for the EFT framework explaining the suppression of the linear term in c_6/Λ^2 still hold.

In Fig. 4.9 are reported the cross sections in the SM and for NP2 in two, three and four boson production respectively.

Multi-Higgs production

In the κ framework, the Higgs interacts with the muon only via Yukawa-like interaction, as the vertices V_2 and V_3 are 0. However, having set $\kappa_\mu = 0$, the modified Yukawa vertex y_μ^{NP} is 0, suggesting that the total cross section $\sigma(\mu^- \mu^+ \rightarrow n h)$ is 0 itself.

This is almost true, but a small caveat has to be made. Indeed, this is actually true only for NPall, when we keep all terms in the new physics expansion of the squared amplitude. However, when we truncate the expansion at a fixed order in c_6 , this is no longer true:

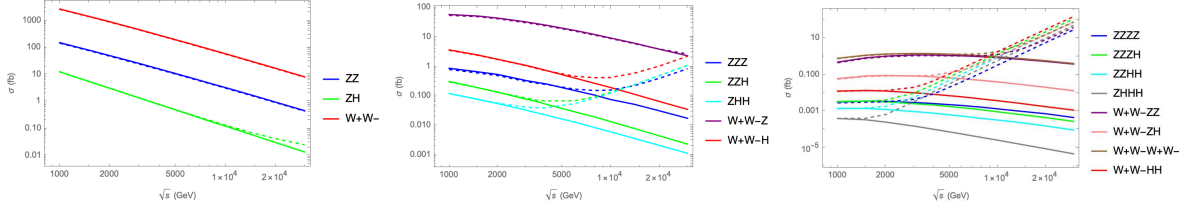


Figure 4.9: Cross section (in fb) for two, three and four boson production in the κ framework, NP2 (dashed lines) and in the SM (solid lines), as functions of \sqrt{s} (GeV).

for $\kappa_\mu = 1 + \delta$, where $\delta \sim c_6$, $\kappa_\mu = 0 \iff \delta = -1$, the new physics expansion is

$$\begin{aligned}
|\mathcal{M}|^2 &= \kappa_\mu A + \kappa_\mu^2 B + \kappa_\mu^3 C + \dots \\
&= (1 + \delta)A + (1 + 2\delta + \delta^2)B + (1 + 3\delta + 3\delta^2 + \delta^3)C + \dots \\
&= (A + B + C + \dots) + \delta(A + 2B + 3C + \dots) + \\
&\quad \delta^2(B + 3C + \dots) + \delta^3(C + \dots) + \dots
\end{aligned} \tag{4.40}$$

Since the coefficients of the powers of δ considered cannot be all 0, the truncated expansion is in general $\neq 0$. This is why the values for $\sigma(\mu^- \mu^+ \rightarrow n h)$ in the NP2 case, shown in Table 4.9, are very small but not exactly 0.

Conclusions

In this thesis we have studied the sensitivity on the muon Yukawa coupling in multiboson production processes at a high-energy muon collider.

We have examined two possible parametrizations of the deviation, the SMEFT and the κ framework, which despite its numerous flaws, is still typically used in the experimental analyses of the Higgs couplings. In the SMEFT formalism we have considered a dimension-6 operator inducing an anomalous Yukawa coupling. Considering the same deviation on the Yukawa coupling in the κ framework, we have shown how it can be interpreted as a higher-dimensional effective field theory. Then, with the Mathematica package FeynRules, we have implemented the SMEFT and κ frameworks into two models, and used them to perform cross section simulations with the event-generator MADGRAPH5_AMC@NLO.

We have then considered the multiboson production processes via muon-antimuon annihilation in the SMEFT and κ formalisms. Thanks to the energy enhancement induced by the violation of unitarity, these processes are particularly suited for precision studies in the multi-Tev energy range.

For these processes, we have analysed the perturbative expansion in the effective coupling: the linear contribution, despite being generally the most meaningful choice due to its unambiguity, is not a good approximation when considering muon annihilation, since it is negligible because of certain suppressions in the polarized amplitudes. Therefore we have considered the second order expansion and shown that higher-order corrections are effectively negligible.

Using the Goldstone Boson Equivalence theorem we have studied analytically the asymptotic energy growth of the multiboson production cross sections in the SMEFT. This first analysis suggests that diboson production is not a suitable process for spotting effects from an anomalous muon Yukawa coupling.

Finally, we have compared for all the processes how the cross sections scale in the SM and in the EFT (or in the κ framework), assuming a 100% deviation of the muon Yukawa from its nominal value. Considering the processes with at least one vector boson produced, in the κ framework we observe for three and in particular four bosons a considerably stronger growth with respect to the SMEFT case. On the contrary, for purely-Higgs final states the cross section is very small in the κ framework, while it is extremely

sensitive to deviations in the SMEFT. In particular, for the triple Higgs case the cross section becomes comparable to other triboson production processes, as expected by the Goldstone Boson Equivalence theorem.

Further studies have to be made, including for example perturbative electroweak corrections that could affect the sensitivity. Moreover, this channel could be a portal for the simultaneous study of the Higgs self coupling and muon Yukawa coupling. In conclusion, the triple Higgs production could be a good observable to detect BSM effects in the multi-TeV range, opening interesting prospects on Higgs precision measurements.

Appendix

The Tables show some values of cross sections for two, three and four boson production in the SM, EFT and κ frameworks, within a center-of-mass energy range of $1 < \sqrt{s} < 30$ TeV. The simulations were carried out in MADGRAPH, with new physics parameters $c_6 = 0.01$ and $\Lambda = 1$ TeV, corresponding to $\kappa_\mu = 0$ according to eq. (4.5).

Standard Model

\sqrt{s} (TeV)	1	2	4	10	20	30	
$ZZZZ$	3.278	3.538	2.668	1.381	0.7459	0.4607	$\cdot 10^{-6}$
$ZZZh$	3.49	3.32	2.223	0.9488	0.4589	0.2822	$\cdot 10^{-6}$
$ZZhh$	14.65	12.7	7.953	3.36	1.598	0.9606	$\cdot 10^{-7}$
$Zhhh$	40.87	25.92	10.47	2.684	0.9065	0.4758	$\cdot 10^{-8}$
W^+W^-ZZ	4.934	10.53	12.02	8.711	5.429	3.871	$\cdot 10^{-4}$
W^+W^-Zh	6.196	9.21	7.746	4.094	2.09	1.337	$\cdot 10^{-5}$
$W^+W^-W^+W^-$	8.039	13.77	14.4	9.86	5.95	4.16	$\cdot 10^{-4}$
W^+W^-hh	12.95	12.99	8.549	3.843	1.814	1.172	$\cdot 10^{-6}$
$hhhh$	26.9	8.133	1.53	0.1564	0.03109	0.01264	$\cdot 10^{-13}$
ZZZ	8.795	5.418	2.572	0.7606	0.3155	0.1744	$\cdot 10^{-4}$
ZZh	3.138	1.359	0.5239	0.1355	0.04433	0.0232	$\cdot 10^{-4}$
Zhh	121.6	55.24	22.44	6.044	2.107	1.13	$\cdot 10^{-6}$
W^+W^-Z	5.887	4.455	2.55	0.937	0.3917	0.233	$\cdot 10^{-2}$
W^+W^-h	37.05	17.71	7.353	1.946	0.6551	0.3505	$\cdot 10^{-4}$
hhh	39.32	7.454	1.588	0.2263	0.05581	0.02547	$\cdot 10^{-11}$
ZZ	15.27	5.069	1.605	0.3306	0.09607	0.04603	$\cdot 10^{-2}$
Zh	12.77	3.144	0.7754	0.1239	0.03073	0.01363	$\cdot 10^{-3}$
W^+W^-	268.4	91.01	28.61	5.909	1.717	0.8276	$\cdot 10^{-2}$
hh	1292	81.13	5.006	0.1327	0.008611	0.001852	$\cdot 10^{-11}$

Table 4.7: Total cross sections (in pb) for the production of two, three and four bosons in the SM, for six values of CM energy.

EFT framework

\sqrt{s} (TeV)	1	2	4	10	20	30	
$ZZZZ$	2.896	3.115	2.466	3.05	11.49	31.2	$\cdot 10^{-6}$
$ZZZh$	3.29	3.242	2.896	11.24	62.35	175.4	$\cdot 10^{-6}$
$ZZhh$	1.429	1.384	1.819	12.35	67.42	181.5	$\cdot 10^{-6}$
$Zhhh$	4.125	2.877	2.699	18.68	107.1	306.2	$\cdot 10^{-7}$
W^+W^-ZZ	4.571	9.689	10.99	8.317	6.398	7.581	$\cdot 10^{-4}$
W^+W^-Zh	5.824	8.657	7.465	5.477	11.54	27.55	$\cdot 10^{-5}$
$W^+W^-W^+W^-$	7.752	13.19	13.76	9.498	6.698	6.742	$\cdot 10^{-4}$
W^+W^-hh	1.247	1.258	1.079	2.781	13.73	37.17	$\cdot 10^{-5}$
$hhhh$	0.1045	0.5309	1.559	6.395	20.47	42.45	$\cdot 10^{-7}$
ZZZ	8.012	4.944	2.466	1.595	3.96	8.451	$\cdot 10^{-4}$
ZZh	3.014	1.325	0.5815	0.4882	1.328	2.897	$\cdot 10^{-4}$
Zhh	1.21	0.5524	0.2773	0.3785	1.278	2.782	$\cdot 10^{-4}$
W^+W^-Z	5.517	4.223	2.396	0.8989	0.4008	0.2714	$\cdot 10^{-2}$
W^+W^-h	3.572	1.737	0.702	0.2541	0.3276	0.609	$\cdot 10^{-3}$
hhh	0.1523	0.4793	1.641	9.44	36.62	82.26	$\cdot 10^{-5}$
ZZ	14.57	4.84	1.534	0.3152	0.09238	0.04454	$\cdot 10^{-2}$
Zh	127.8	31.06	7.734	1.345	0.4266	0.2503	$\cdot 10^{-4}$
W^+W^-	261.7	88.47	27.94	5.739	1.67	0.8056	$\cdot 10^{-2}$
hh	5.161	5.254	5.301	5.305	5.296	5.294	$\cdot 10^{-5}$

Table 4.8: Total cross sections (in pb) for the production of two, three and four bosons at second order (NP2) in the EFT, for six values of CM energy.

κ framework

\sqrt{s} (TeV)	1	2	4	10	20	30	
$ZZZZ$	0.02898	0.03346	0.09069	3.363	57.18	290.2	$\cdot 10^{-4}$
$ZZZh$	0.033	0.04182	0.2973	13.42	222.2	1148	$\cdot 10^{-4}$
$ZZhh$	0.01418	0.01874	0.1892	8.897	150.4	771.2	$\cdot 10^{-4}$
$Zhhh$	0.004136	0.00672	0.1217	5.948	98.41	507.8	$\cdot 10^{-4}$
W^+W^-ZZ	4.571	9.689	11.05	12.76	81.4	391.2	$\cdot 10^{-4}$
W^+W^-Zh	0.5824	0.8736	0.9494	9.709	152.5	773.7	$\cdot 10^{-4}$
$W^+W^-W^+W^-$	7.753	13.22	13.89	18.38	157	776.5	$\cdot 10^{-4}$
W^+W^-hh	0.1244	0.137	0.4771	18.32	301.9	1540	$\cdot 10^{-4}$
$hhhh$	17.45	25.74	12.85	3.675	1.123	0.6796	$\cdot 10^{-19}$
ZZZ	8.012	4.944	2.466	1.594	3.977	8.455	$\cdot 10^{-4}$
ZZh	3.009	1.335	0.6817	1.331	4.878	11.15	$\cdot 10^{-4}$
Zhh	1.21	0.5722	0.3988	1.251	4.932	10.96	$\cdot 10^{-4}$
W^+W^-Z	55.17	42.23	23.97	8.988	3.954	2.693	$\cdot 10^{-3}$
W^+W^-h	3.571	1.739	0.7236	0.4261	1.038	2.252	$\cdot 10^{-3}$
hhh	100	53.79	18.99	4.04	1.176	0.6304	$\cdot 10^{-17}$
ZZ	14.57	4.84	1.534	0.3152	0.09238	0.04454	$\cdot 10^{-2}$
Zh	127.8	31.306	7.734	1.345	0.4266	0.2503	$\cdot 10^{-4}$
W^+W^-	261.8	88.47	27.94	5.739	1.67	0.8056	$\cdot 10^{-2}$
hh	67.34	25.82	9.009	1.888	0.5731	0.2795	$\cdot 10^{-14}$

Table 4.9: Total cross sections (in pb) for the production of two, three and four bosons at second order (NP2) in the κ framework, for six values of CM energy.

Acknowledgments

I would like to express my deep gratitude to my supervisors, Professors Davide Pagani and Fabio Maltoni, for their fundamental contribution to the development of this work and for their constant support during this year.

I am particularly thankful to Davide Pagani for the great deal of patience and time he spent over this work. Our discussions have always been extremely helpful and inspiring. It is not an overstatement to say that this thesis would not have been possible without his ideas and his guidance.

I would also like to thank Fabio Maltoni, who gave the original input for this project, for providing a lot of insightful ideas and for giving me the opportunity to spend some months at the CP3 (*Centre for Cosmology, Particle Physics and Phenomenology*). During this incredible experience I met a lot of amazing people and learned first-hand what it means to be a researcher.

Bibliography

- [1] ATLAS collaboration. “Observation of a new particle in the search for the Standard Model Higgs boson with the ATLAS detector at the LHC”. In: *Physics Letters B* 716.1 (2012). ISSN: 0370-2693. DOI: <https://doi.org/10.1016/j.physletb.2012.08.020>.
- [2] CMS collaboration. “Observation of a new boson at a mass of 125 GeV with the CMS experiment at the LHC”. In: *Physics Letters B* 716.1 (2012). ISSN: 0370-2693. DOI: <https://doi.org/10.1016/j.physletb.2012.08.021>.
- [3] A. M. Sirunyan et al. “Evidence for Higgs boson decay to a pair of muons”. In: *Journal of High Energy Physics* 2021.1 (2021). DOI: [10.1007/JHEP01\(2021\)148](https://doi.org/10.1007/JHEP01(2021)148).
- [4] ATLAS collaboration. “A search for the dimuon decay of the Standard Model Higgs boson with the ATLAS detector”. In: *Physics Letters B* 812 (2021). ISSN: 0370-2693. DOI: <https://doi.org/10.1016/j.physletb.2020.135980>.
- [5] John M. Cornwall, David N. Levin, and George Tiktopoulos. “Derivation of Gauge Invariance from High-Energy Unitarity Bounds on the s Matrix”. In: *Phys. Rev. D* 10 (1974). [Erratum: *Phys.Rev.D* 11, 972 (1975)]. DOI: [10.1103/PhysRevD.10.1145](https://doi.org/10.1103/PhysRevD.10.1145).
- [6] T. Appelquist and Michael S. Chanowitz. “Unitarity Bound on the Scale of Fermion Mass Generation”. In: *Phys. Rev. Lett.* 59 (1987). [Erratum: *Phys.Rev.Lett.* 60, 1589 (1988)]. DOI: [10.1103/PhysRevLett.59.2405](https://doi.org/10.1103/PhysRevLett.59.2405).
- [7] M.E. Peskin and D.V. Schroeder. *An Introduction to Quantum Field Theory*. Westview Press, 2016.
- [8] ATLAS collaboration. *Projections for measurements of Higgs boson cross sections, branching ratios, coupling parameters and mass with the ATLAS detector at the HL-LHC*. Tech. rep. CERN, 2018. URL: <https://cds.cern.ch/record/2652762>.
- [9] CMS collaboration. *Sensitivity projections for Higgs boson properties measurements at the HL-LHC*. Tech. rep. CERN, 2018. URL: <https://cds.cern.ch/record/2647699>.
- [10] European Strategy For Particle Physics Preparatory Group. *Physics Briefing Book*. 2019. DOI: [10.48550/ARXIV.1910.11775](https://doi.org/10.48550/ARXIV.1910.11775).
- [11] J. de Blas et al. “Higgs Boson studies at future particle colliders”. In: *Journal of High Energy Physics* 2020.1 (2020). DOI: [10.1007/JHEP01\(2020\)139](https://doi.org/10.1007/JHEP01(2020)139).

- [12] Howard Baer et al. *The International Linear Collider Technical Design Report - Volume 2: Physics*. DOI: [10.48550/ARXIV.1306.6352](https://doi.org/10.48550/ARXIV.1306.6352).
- [13] Ties Behnke et al. *The International Linear Collider Technical Design Report - Volume 4: Detectors*. 2013. DOI: [10.48550/ARXIV.1306.6329](https://doi.org/10.48550/ARXIV.1306.6329).
- [14] FCC collaboration. “FCC-ee: The Lepton Collider”. In: *The European Physical Journal Special Topics* 228.2 (2019). DOI: [10.1140/epjst/e2019-900045-4](https://doi.org/10.1140/epjst/e2019-900045-4).
- [15] The CEPC Study Group. *CEPC Conceptual Design Report: Volume 2 - Physics & Detector*. 2018. DOI: [10.48550/ARXIV.1811.10545](https://doi.org/10.48550/ARXIV.1811.10545).
- [16] Geneva CERN. *CERN Yellow Reports, Vol 4 (2016): Updated Baseline for a staged Compact Linear Collider*. 2016. DOI: [10.5170/CERN-2016-004](https://doi.org/10.5170/CERN-2016-004).
- [17] FCC collaboration. “FCC Physics Opportunities”. In: *The European Physical Journal C* 79.6 (2019). DOI: [10.1140/epjc/s10052-019-6904-3](https://doi.org/10.1140/epjc/s10052-019-6904-3).
- [18] T. Aoyama et al. “The anomalous magnetic moment of the muon in the Standard Model”. In: *Physics Reports* 887 (2020). ISSN: 0370-1573.
- [19] Muon $g - 2$ collaboration. “Final report of the E821 muon anomalous magnetic moment measurement at BNL”. In: *Phys. Rev. D* 73 (7 Apr. 2006).
- [20] Muon $g - 2$ collaboration. “Measurement of the Positive Muon Anomalous Magnetic Moment to 0.46 ppm”. In: *Phys. Rev. Lett.* 126 (14 Apr. 2021).
- [21] Sz. Borsanyi et al. “Leading hadronic contribution to the muon magnetic moment from lattice QCD”. In: *Nature* 593.7857 (2021). DOI: [10.1038/s41586-021-03418-1](https://doi.org/10.1038/s41586-021-03418-1).
- [22] LHCb collaboration. “Test of lepton universality in beauty-quark decays”. In: *Nature Physics* 18.3 (2022). DOI: [10.1038/s41567-021-01478-8](https://doi.org/10.1038/s41567-021-01478-8).
- [23] Sébastien Descotes-Genon et al. “Global analysis of $b \rightarrow sll$ anomalies”. In: *Journal of High Energy Physics* 2016.6 (2016). DOI: [10.1007/JHEP06\(2016\)092](https://doi.org/10.1007/JHEP06(2016)092).
- [24] Marzia Bordone, Gino Isidori, and Andrea Pattori. “On the standard model predictions for R_K and R_{K^*} ”. In: *The European Physical Journal C* 76.8 (2016). DOI: [10.1140/epjc/s10052-016-4274-7](https://doi.org/10.1140/epjc/s10052-016-4274-7).
- [25] Christoph Bobeth, Gudrun Hiller, and Giorgi Piranishvili. “Angular distributions of $\bar{B} \rightarrow K\bar{l}l$ decays”. In: *Journal of High Energy Physics* 2007.12 (Dec. 2007). DOI: [10.1088/1126-6708/2007/12/040](https://doi.org/10.1088/1126-6708/2007/12/040).
- [26] J. P. Delahaye et al. *Muon Colliders*. 2019. DOI: [10.48550/ARXIV.1901.06150](https://doi.org/10.48550/ARXIV.1901.06150).
- [27] N. Bartosik et al. “Detector and Physics Performance at a Muon Collider”. In: *Journal of Instrumentation* 15.05 (May 2020). DOI: [10.1088/1748-0221/15/05/p05001](https://doi.org/10.1088/1748-0221/15/05/p05001).
- [28] Daniel Schulte et al. “Prospects on Muon Colliders”. In: *PoS ICHEP2020* (2021). DOI: [10.22323/1.390.0703](https://doi.org/10.22323/1.390.0703).

- [29] Jorge de Blas, Jiayin Gu, and Zhen Liu. *Higgs Precision at a 125 GeV Muon Collider*. 2022. arXiv: [2203.04324](https://arxiv.org/abs/2203.04324) [[hep-ph](#)].
- [30] C. Aimè et al. *Muon Collider Physics Summary*. 2022. arXiv: [2203.07256](https://arxiv.org/abs/2203.07256) [[hep-ph](#)].
- [31] A. V. Manohar. *Introduction to Effective Field Theories*. 2018.
- [32] T. Appelquist and J. Carazzone. “Infrared singularities and massive fields”. In: *Phys. Rev. D* 11 (10 May 1975). DOI: [10.1103/PhysRevD.11.2856](https://doi.org/10.1103/PhysRevD.11.2856).
- [33] Witold Skiba. *TASI Lectures on Effective Field Theory and Precision Electroweak Measurements*. 2010. DOI: [10.48550/ARXIV.1006.2142](https://doi.org/10.48550/ARXIV.1006.2142).
- [34] A. Pich. *Effective Field Theory*. 1998. DOI: [10.48550/ARXIV.HEP-PH/9806303](https://doi.org/10.48550/ARXIV.HEP-PH/9806303).
- [35] B. Grzadkowski et al. “Dimension-six terms in the Standard Model Lagrangian”. In: *Journal of High Energy Physics* 2010.10 (2010). DOI: [10.1007/JHEP10\(2010\)085](https://doi.org/10.1007/JHEP10(2010)085).
- [36] Tao Han et al. “Precision test of the muon-Higgs coupling at a high-energy muon collider”. In: *Journal of High Energy Physics* 2021.12 (2021).
- [37] Adam Falkowski et al. “Light quark Yukawas in triboson final states”. In: *JHEP* 04 (2021). DOI: [10.1007/JHEP04\(2021\)023](https://doi.org/10.1007/JHEP04(2021)023). arXiv: [2011.09551](https://arxiv.org/abs/2011.09551) [[hep-ph](#)].
- [38] Brian Henning et al. “Measuring Higgs Couplings without Higgs Bosons”. In: *Phys. Rev. Lett.* 123 (18 Oct. 2019). DOI: [10.1103/PhysRevLett.123.181801](https://doi.org/10.1103/PhysRevLett.123.181801).